Elsevier Editorial System(tm) for Chemical Engineering Journal

Manuscript Draft

Manuscript Number: CEJ-D-16-01044R2

Title: Using an experimentally-determined model of the evolution of pore structure for the calcination of cycled limestones

Article Type: Research Paper

Keywords: Calcium looping; Modelling; Calcination; Pore evolution

Corresponding Author: Mr. Peng Dai,

Corresponding Author's Institution: University of Cambridge

First Author: Peng Dai

Order of Authors: Peng Dai; Belén González; John S Dennis

Abstract: A pseudo-steady state model of reaction and diffusion has been constructed to model the non-isothermal calcination of limestone particles which have been subjected to a history of cycling between the calcined and carbonated states. This typically occurs when using Ca-based materials for removing CO2 from the flue gas of plants such as a power station, cement plant and steel factory in certain schemes for carbon capture and storage. The model uses a Cylindrical Pore Interpolation Model to describe the intraparticle mass transfer of CO2 through the pores of the material coupled with an experimentally-determined function, f(X), describing the pore evolution as a function of the conversion of the CaCO3 present to CaO. The intrinsic rate of calcination was taken to be first order in concentration driving force. External to the limestone particle, the Stefan-Maxwell equations were used to describe the diffusion of CO2 away from the particle and into the particulate phase of the fluidised bed. The equation of energy was used to allow for the enthalpy of the reaction. In order to validate the use of the f(X) function, the theoretical predictions were compared with experiments conducted to measure the rates and extent of conversion, at various temperature and different particle sizes, of Purbeck and Compostilla limestones that had been previously cycled between the carbonated and fully-calcined state. Excellent agreement between experiment and theory was obtained, and the model using the f(X) approach predicted the conversion of particles of various sizes well at temperatures different to that at which the function was derived, thus indicating that the f(X) solely dependent on the evolution of the morphology of the particle.

Response to Reviewers: All related changes are highlighted in the text when it is possible.

Reviewer 1
Issue 1
In answering issue 1 of referee 1, the authors state "However, in his model the small pore trees will be kinetically limited while the larger pore trees are diffusion limited. This is the opposite of what one would normally expect."

I disagree with this statement. If the small trees have significant diffusion resistance, the larger trees having much larger length scales will have much stronger diffusion limitations, and the particle scale Thiele modulus will be very large. The authors may read the text of Bischoff and Froment for a discussion of this aspect with regard to micropore and macropore diffusion limitations.
Response
The text on page 6 now reads:
“However, in his model the small pore trees will be kinetically limited while the larger pore trees are diffusion limited. This is the opposite of one might expect for pores with uniform length.”

Issue 2
The authors next state "The existing mathematical pore models such as the random pore model, the pore tree model and the grain model have various degrees of mathematical complexity, but, more importantly, contain one or more unknown parameters which have to be fitted to experimental results." I cannot agree completely with this. For example the structural parameter of the Random Pore Model can be independently estimated from the pore size distribution.
Response
The text on page 6 now reads:
“The existing mathematical pore models such as the random pore model, statistical pore tree model and grain model contain parameters that are difficult to measure and thus become fitting parameters, e.g. the diffusivity of SO2 through a layer of CaSO4, which are complicated and equally arbitrary. In many cases, the use of mathematical pore models leads to the need to modify the original models in order to fit experimental measurements [9-11].”

Issue 3
While I do not want to insist on fitting of their rate curve to a mechanism, it remains a weakness if they do not do so. While such fitting does have parameters, in most cases they can be reconciled with existing literature information obtained in a different context or experiment. By providing such mechanistic interpretation the authors could strengthen the paper and its appeal.
Response
The referee’s point is taken and will be thoroughly considered in the subsequent study where we will apply the model to simulating the sulphation of limestones where there are two different mechanisms for the reaction to terminate depending on temperature. This is where our model could be very useful in determining which mechanism the reaction would follow and when the transition would occur. However, the purpose of this study was to verify experimentally the continuous reaction model using the f(X) concept, originally developed and verified for gasification of chars, to describe the evolution of pores. Therefore, the primary objective of this paper is to communicate fully the features associated with the theoretical model and to demonstrate the applicability to a distinctively different gas-solid reaction other than the gasification of chars reported previously.

Reviewer 3
Issue 1 – Introduction

Although some new references have been included in the introduction, more references are required to support some statements in the introduction. Examples are:
1. Page 5: "The SCM has been commonly used to describe, for example, the calcination of non-porous, virgin particles of limestone…, where the reaction occurs at a sharp front which recedes towards the centre of the particles".
2. Page 5: "The calcination of cycled, as opposed to virgin limestone, possesses the characteristics of the CRM…".
3. Page 5: "A feature of most models of non-catalytic reactions between gases and solids generally is that the intrinsic rate of reaction, r, at a local point within a solid particle is of the form $r=g(Ci, T, P)\cdot f(X)$".
4. Page 7: "However, limestones which have been successively calcined to CaO and carbonated in CO2 back to CaCO3, many times, present a different type of porous solid…".
5. The comment in the first review saying that "also fixed bed reactors use particles that cycle between carbonation and calcination states" was meant to highlight that other types of reactors or devices can be used to calcine limestone (TGA, oven…). Therefore, I suggest deleting "in a fluidised bed or a fixed bed reactor" from the sentence in page 5: "such particles are created when raw limestone particles have been subjected to a history of cycling between the calcined and carbonated states in a fluidised bed or a fixed bed reactor" to make it more general.
Response
1. Reference [1] is added on page 5.
2. This statement does not need a reference because cycled limestones are much more porous than the virgin limestones, hence the calcination would occurs across the entire particle rather than on a sharp front as shown in Fig. 1. Thus no change has been made.
3. Reference [2,3] is added on page 5.
4. Same as issue 2, where the cycled limestones become porous thus allowing reaction to occur through the entire particle. Hence no change has been made.
5. The text now read:
"Such particles are created when raw limestone particles have been subjected to a history of cycling between the calcined and carbonated states."

Issue 2 - Experimental
1. Page 7: the authors justified why they chose a different number of cycles for each limestone, but should also mention that the reason why they chose cycled particles is to ensure that the solid is porous. Besides, they included this statement: "The number of cycles was chosen so that the ultimate CO2 uptake by the limestones of the current cycle was close to that of the previous cycle". Does this means that particles are in their residual activity? If so, why it is achieved in so less cycles?
2. Page 9: authors included that "From experimental measurements using different sample masses, a sample mass of 0.30 g limestone added to the bed was chosen to avoid complications arising from mass transfer between the bubble and the particulate phases". Authors should discuss more about this, indicating the sample masses used and the results obtained that led to the selection of the 0.30 g mass.
3. Page 9: "To ensure complete calcination of the limestones, experiment is ended 10 seconds after the measure concentration of CO2 of the off-gas returns to zero". I think what they refer to is to the end of the calcination stage, not of the experiment.
Response

1. The text on page 7 now reads:
“The number of cycles was chosen so that the particles become porous and the ultimate CO2 uptake by the limestones of the current cycle was close to that of the previous cycle.”
2. The text on page 9 now reads:
“From experimental measurements using different sample masses ranging from 0.1 – 0.5 g at 1173 K, the measurement of reaction rate starts decreased when the sample mass was bigger than 0.3 g due to complications arising from mass transfer between the bubble and the particulate phases. Hence a sample mass of 0.3 g was chose for all experiments”
3. The text on page 9 now reads:
“To ensure complete calcination of the limestones, the calcination experiment is ended 10 seconds after the measured concentration of CO2 of the off-gas returns to zero.”

Issue 3 – Theoretical
1. Page 11: indicate the units of temperature (K) in equation 4.
2. Page 12: replace ya for yn in the last paragraph.
3. References for equations 15, 19, 22 should be given. Also, reference for the equation included in page 15, line 6 should be mentioned.
4. Page 15: the hmf is 0.029 m. How was it determined (visually?)?
5. Reference for equation included in page 16, lines 4-5.
Response
1. The following text is added below Eq. 4:
“where the unit of T is in K.”
2. The text on page 12 now reads:
“Here, yn is the mole fraction of species n”
3. References [24,28], [26] and [26] are added to Eq. 15, 19 and 22 respectively. The equation included in page 15 line 6 is a derived one from mass balance hence no reference is required.
4. It was measured when the bed is taken out of the furnace and fully fluidised at room temperature.
5. The reference [27] has already been given in the text. Thus no change is made.

Issue 4 – Results
1. The cycle number of the particles in Figure 3 should be mentioned.
2. I still think that talking about figures 5 and 8 in page 18 (before showing even figure 4) makes the paper hard to read, as they are in subsequent sections and not in the section where they are mentioned. As authors note, it is true that the editorial team will decide where the figures will be place, but they tend to maintain the order selected by the authors. I suggest addressing this issue.
3. The cycle number of the particles in figures 4, 5, 6 and 8 should be indicated.
4. Figure 6 shows a normalized dX/dt, but it is higher than 1.
5. Page 20: "…was able to fit well the experimental results at 1023 K, as seen in Fig. 5(a)". Fig. 5(a) should be replaced by Fig. 7(a).
Response
1. The cycle numbers are added in the caption of Fig. 3, the text now reads:
“Fig. 3. Measurements of CO2 mole fraction during calcination of cycled limestones at atmospheric pressure: a) Compostilla 8 cycles 0.71 – 0.85 mm at 1173 K; b) Purbeck 6 cycles 0.71 – 0.85 mm at 1173 K.”
2. We understand the reviewer’s concern on the current arrangement of Fig. 5 and Fig. 8, however all the results are presented in the subsection corresponding to the material studied. We still believe the current arrangement provides a smooth read, after explicitly mentioning

the location of the figures (in section 4.1 and 4.2 respectively). The text on page 18 now reads: “The linearity of Fig. 5 and Fig. 8 in section 4.1 and 4.2 respectively show that the calcination of the limestone was indeed controlled by chemical kinetics at low temperature, hence confirming the use of Eq. (29) for the determination of the kinetic parameters.”
3. The cycle numbers are added to the captions of Fig. 4, 5, 6 and 8.
4. Fig. 6 uses normalised plot of rate against conversion to determine the f(X) function. The result shows a peak at about 20% conversion and higher than 1. This is due to the fact that as the limestone particle calcines, part of the surface area that is previously unreachable become accessible when the solid volume reduces during calcination. This increase in surface area only occurs at low conversion when the coalescence of pores is insignificant. The following text is added on page 20:
“The figure shows a peak higher than 1 at about 20% conversion. This is due to the fact that part of the surface area that is previously unreachable become accessible when the solid volume reduces during the initial stage of calcination. This increase in surface area only occurs at low conversion when the coalescence of pores is insignificant.”
5. The text on page 20 now reads:
“Using this f(X), the model was able to fit well the experimental results at 1023 K, as seen in Fig. 7(a).”

Issue 5 – Discussion
Page 23: "Thus, the intrinsic rate of carbonation changes little with temperature". This is true in the temperature range analysed in the paper.
Response
The text on page 23 now read:
“Thus, the intrinsic rate of carbonation changes little with temperature in the temperature range studied in the paper.”

Department of Chemical Engineering and Biotechnology
University of Cambridge
New Museums Site
Pembroke Street
Cambridge CB2 3RA
United Kingdom

11 February 2016

Editorial office
Chemical Engineering Journal

Dear Editor,

Original Research Paper for Consideration by *Chemical Engineering Journal*

Please find attached an original research paper, which we would like to be considered for publication in *Chemical Engineering Journal*. It presents a new method of modelling the rate of calcination of particles of limestone, in which the key improvement is to determine the parameter affecting pore morphology experimentally, rather than using artificial models of pore structure to infer how the morphology evolves with reaction. The model has been compared with experiments at various conditions and appears to be a robust predictor of rate of reaction and conversion versus time.

We have prepared this manuscript according to Guide for Authors and in compliance with the Ethics in Publishing Policy as described in the Guide for Authors. We also confirm that:

- This is an original submission by the authors and has not been submitted for publication elsewhere.
- The list of suggested reviewers with their contact details are attached in a separate document.
- Keywords are provided.
- References are in the correct format.
- The PDF of the manuscript is in correct order upon submission.
- The length of the manuscript is in compliance with the Guide for Authors.

We thank you for considering this manuscript for publication.

Yours sincerely,

Peng Dai

(On behalf of all the co-authors)

***List of Suggested Reviewers**

First name	Maria
Last name	Diego
Degree	PhD
Position	Postdoc
Department	Coal, Energy and Environment
Institution	Instituto Nacional del Carbón
Email	marlen@incar.csic.es
Reasons: Dr Diego has extensive research contributions on calcium looping process for CO2 capture, where her work spans from fundamental studies of the reaction kinetics and circulating fluidised bed to investigations of the large scale calcium looping pilot plant.	

First name	Marcin
Last name	Broda
Degree	PhD
Position	Postdoc
Department	Institute of Energy Technology
Institution	Eidgenossische Technische Hochschule Zurich
Email	mbroda@student.ethz.ch
Reasons: Dr Broda has a long list of publications on calcium looping process where he worked extensively on the studies of the synthetic Ca-based sorbents and their performance in the looping process.	

First name	Vasilije
Last name	Manovic
Degree	PhD
Position	Professor
Department	Energy and Power Engineering Division, School of Engineering
Institution	Cranfield University
Email	v.manovic@cranfield.ac.uk
Reasons: Professor Manovic is a leading authority in the area of calcium looping – a new technology for CO2 capture, and he is an internationally recognised authority in several other CO2 capture areas including chemical looping combustion, oxy-fuel combustion, and CO2 capture from low-CO2-concentration sources such as industrial gases, natural gas, and air. His research interests also include the areas of SO2 capture, NOx reduction from fossil fuel, biomass, and waste combustion. He has also studied pyrolysis, and gasification, and been responsible for the modelling of these processes. In addition, his expertise includes chemistry, geochemistry, and analytical chemistry of fossil fuels.	

First name	Ben
Last name	Anthony
Degree	PhD
Position	Professor
Department	Centre for Combustion, Carbon Capture & Storage
Institution	Cranfield University
Email	b.j.anthony@cranfield.ac.uk

Reasons:
Professor Anthony's current R&D pursuits are strongly focused on calcium and chemical looping cycles, oxy-fired Circulating Fluidized Bed Combustion (CFBC) technology and pressurised, entrained-flow gasification.

Response to the comments

All related changes are highlighted in the text when it is possible.

Reviewer 1

Issue 1

In answering issue 1 of referee 1, the authors state "However, in his model the small pore trees will be kinetically limited while the larger pore trees are diffusion limited. This is the opposite of what one would normally expect."

I disagree with this statement. If the small trees have significant diffusion resistance, the larger trees having much larger length scales will have much stronger diffusion limitations, and the particle scale Thiele modulus will be very large. The authors may read the text of Bischoff and Froment for a discussion of this aspect with regard to micropore and macropore diffusion limitations.

Response

The text on page 6 now reads:

“However, in his model the small pore trees will be kinetically limited while the larger pore trees are diffusion limited. This is the opposite of one might expect for pores with uniform length.”

Issue 2

The authors next state "The existing mathematical pore models such as the random pore model, the pore tree model and the grain model have various degrees of mathematical complexity, but, more importantly, contain one or more unknown parameters which have to be fitted to experimental results."

I cannot agree completely with this. For example the structural parameter of the Random Pore Model can be independently estimated from the pore size distribution.

Response

The text on page 6 now reads:

“The existing mathematical pore models such as the random pore model, statistical pore tree model and grain model contain parameters that are difficult to measure and thus become fitting parameters, *e.g.* the diffusivity of SO_2 through a layer of $CaSO_4$, which are complicated and equally arbitrary. In many cases, the use of

mathematical pore models leads to the need to modify the original models in order to fit experimental measurements [9-11].”

Issue 3

While I do not want to insist on fitting of their rate curve to a mechanism, it remains a weakness if they do not do so. While such fitting does have parameters, in most cases they can be reconciled with existing literature information obtained in a different context or experiment. By providing such mechanistic interpretation the authors could strengthen the paper and its appeal.

Response

The referee’s point is taken and will be thoroughly considered in the subsequent study where we will apply the model to simulating the sulphation of limestones where there are two different mechanisms for the reaction to terminate depending on temperature. This is where our model could be very useful in determining which mechanism the reaction would follow and when the transition would occur. However, the purpose of this study was to verify experimentally the continuous reaction model using the $f(X)$ concept, originally developed and verified for gasification of chars, to describe the evolution of pores. Therefore, the primary objective of this paper is to communicate fully the features associated with the theoretical model and to demonstrate the applicability to a distinctively different gas-solid reaction other than the gasification of chars reported previously.

Reviewer 3

Issue 1 – Introduction

Although some new references have been included in the introduction, more references are required to support some statements in the introduction. Examples are:

1. Page 5: "The SCM has been commonly used to describe, for example, the calcination of non-porous, virgin particles of limestone…, where the reaction occurs at a sharp front which recedes towards the centre of the particles".
2. Page 5: "The calcination of cycled, as opposed to virgin limestone, possesses the characteristics of the CRM…".
3. Page 5: "A feature of most models of non-catalytic reactions between gases and solids generally is that the intrinsic rate of reaction, r, at a local point within a solid particle is of the form $r=g(Ci, T, P)\cdot f(X)$".
4. Page 7: "However, limestones which have been successively calcined to CaO and carbonated in CO2 back to CaCO3, many times, present a different type of porous solid…".
5. The comment in the first review saying that "also fixed bed reactors use particles that cycle between carbonation and calcination states" was meant to highlight that other types of reactors or devices can be used to calcine limestone (TGA, oven…). Therefore, I suggest deleting "in a fluidised bed or a fixed bed reactor" from the sentence in page 5: "such particles are created when raw limestone particles have been subjected to a history of cycling between the calcined and carbonated states in a fluidised bed or a fixed bed reactor" to make it more general.

Response

1. Reference [1] is added on page 5.
2. This statement does not need a reference because cycled limestones are much more porous than the virgin limestones, hence the calcination would occurs across the entire particle rather than on a sharp front as shown in Fig. 1. Thus no change has been made.
3. Reference [2,3] is added on page 5.
4. Same as issue 2, where the cycled limestones become porous thus allowing reaction to occur through the entire particle. Hence no change has been made.
5. The text now read:

   “Such particles are created when raw limestone particles have been subjected to a history of cycling between the calcined and carbonated states.”

Issue 2 - Experimental

1. Page 7: the authors justified why they chose a different number of cycles for each limestone, but should also mention that the reason why they chose cycled particles is to ensure that the solid is porous. Besides, they included this statement: "The number of cycles was chosen so that the ultimate CO2 uptake by the limestones of the current cycle was close to that of the previous cycle". Does this means that particles are in their residual activity? If so, why it is achieved in so less cycles?
2. Page 9: authors included that "From experimental measurements using different sample masses, a sample mass of 0.30 g limestone added to the bed was chosen to avoid complications arising from mass transfer between the bubble and the particulate phases". Authors should discuss more about this, indicating the sample masses used and the results obtained that led to the selection of the 0.30 g mass.
3. Page 9: "To ensure complete calcination of the limestones, experiment is ended 10 seconds after the measure concentration of CO2 of the off-gas returns to zero". I think what they refer to is to the end of the calcination stage, not of the experiment.

Response

1. The text on page 7 now reads:

   "The number of cycles was chosen so that the particles become porous and the ultimate CO_2 uptake by the limestones of the current cycle was close to that of the previous cycle."
2. The text on page 9 now reads:

   "From experimental measurements using different sample masses ranging from 0.1 – 0.5 g at 1173 K, the measurement of reaction rate starts decreased when the sample mass was bigger than 0.3 g due to complications arising from mass transfer between the bubble and the particulate phases. Hence a sample mass of 0.3 g was chose for all experiments"
3. The text on page 9 now reads:

   "To ensure complete calcination of the limestones, the calcination experiment is ended 10 seconds after the measured concentration of CO2 of the off-gas returns to zero."

Issue 3 – Theoretical

1. Page 11: indicate the units of temperature (K) in equation 4.
2. Page 12: replace ya for yn in the last paragraph.

3. References for equations 15, 19, 22 should be given. Also, reference for the equation included in page 15, line 6 should be mentioned.
4. Page 15: the hmf is 0.029 m. How was it determined (visually?)?
5. Reference for equation included in page 16, lines 4-5.

Response

1. The following text is added below Eq. 4:

   "where the unit of T is in K."
2. The text on page 12 now reads:

   "Here, y_n is the mole fraction of species n"
3. References [24,28], [26] and [26] are added to Eq. 15, 19 and 22 respectively. The equation included in page 15 line 6 is a derived one from mass balance hence no reference is required.
4. It was measured when the bed is taken out of the furnace and fully fluidised at room temperature.
5. The reference [27] has already been given in the text. Thus no change is made.

Issue 4 – Results

1. The cycle number of the particles in Figure 3 should be mentioned.
2. I still think that talking about figures 5 and 8 in page 18 (before showing even figure 4) makes the paper hard to read, as they are in subsequent sections and not in the section where they are mentioned. As authors note, it is true that the editorial team will decide where the figures will be place, but they tend to maintain the order selected by the authors. I suggest addressing this issue.
3. The cycle number of the particles in figures 4, 5, 6 and 8 should be indicated.
4. Figure 6 shows a normalized dX/dt, but it is higher than 1.
5. Page 20: "…was able to fit well the experimental results at 1023 K, as seen in Fig. 5(a)". Fig. 5(a) should be replaced by Fig. 7(a).

Response

1. The cycle numbers are added in the caption of Fig. 3, the text now reads:

   "Fig. 3. Measurements of CO2 mole fraction during calcination of cycled limestones at atmospheric pressure: a) Compostilla 8 cycles 0.71 – 0.85 mm at 1173 K; b) Purbeck 6 cycles 0.71 – 0.85 mm at 1173 K."

2. We understand the reviewer's concern on the current arrangement of Fig. 5 and Fig. 8, however all the results are presented in the subsection corresponding to the material studied. We still believe the current arrangement provides a smooth read, after explicitly mentioning the location of the figures (in section 4.1 and 4.2 respectively). The text on page 18 now reads: "The linearity of Fig. 5 and Fig. 8 in section 4.1 and 4.2 respectively show that the calcination of the limestone was indeed controlled by chemical kinetics at low temperature, hence confirming the use of Eq. (29) for the determination of the kinetic parameters."
3. The cycle numbers are added to the captions of Fig. 4, 5, 6 and 8.
4. Fig. 6 uses normalised plot of rate against conversion to determine the $f(X)$ function. The result shows a peak at about 20% conversion and higher than 1. This is due to the fact that as the limestone particle calcines, part of the surface area that is previously unreachable become accessible when the solid volume reduces during calcination. This increase in surface area only occurs at low conversion when the coalescence of pores is insignificant. The following text is added on page 20:
   "The figure shows a peak higher than 1 at about 20% conversion. This is due to the fact that part of the surface area that is previously unreachable become accessible when the solid volume reduces during the initial stage of calcination. This increase in surface area only occurs at low conversion when the coalescence of pores is insignificant."
5. The text on page 20 now reads:
   "Using this f(X), the model was able to fit well the experimental results at 1023 K, as seen in Fig. 7(a)."

Issue 5 – Discussion

Page 23: "Thus, the intrinsic rate of carbonation changes little with temperature". This is true in the temperature range analysed in the paper.

Response

The text on page 23 now read:

"Thus, the intrinsic rate of carbonation changes little with temperature in the temperature range studied in the paper."

Highlights

- A pseudo time-stepping model with spatial variation for calcination of cycled limestones.
- An experimentally determined function to describe the evolution of pore structure.
- Good fit between the model and the experimental measurements.

Using an experimentally-determined model of the evolution of pore structure for the calcination of cycled limestones

Peng Dai*, Belén González, John S. Dennis

University of Cambridge, Department of Chemical Engineering and Biotechnology, New Museums Site, Pembroke Street, Cambridge, CB2 3RA, United Kingdom

Corresponding author

* Phone: +44(0)1223 336633. Email: pd337@cam.ac.uk

Abstract

A pseudo-steady state model of reaction and diffusion has been constructed to model the non-isothermal calcination of limestone particles which have been subjected to a history of cycling between the calcined and carbonated states. This typically occurs when using Ca-based materials for removing CO_2 from the flue gas of plants such as a power station, cement plant and steel factory in certain schemes for carbon capture and storage. The model uses a Cylindrical Pore Interpolation Model to describe the intraparticle mass transfer of CO_2 through the pores of the material coupled with an experimentally-determined function, $f(X)$, describing the pore evolution as a function of the conversion of the $CaCO_3$ present to CaO. The intrinsic rate of calcination was taken to be first order in concentration driving force. External to the limestone particle, the Stefan-Maxwell equations were used to describe the diffusion of CO_2 away from the particle and into the particulate phase of the fluidised bed. The equation of energy was used to allow for the enthalpy of the reaction. In order to validate the use of the $f(X)$ function, the theoretical predictions were compared with experiments conducted to measure the rates and extent of conversion, at various temperature and different particle sizes, of Purbeck and Compostilla limestones that had been previously cycled between the carbonated and fully-calcined state. Excellent agreement between experiment and theory was obtained, and the model using the $f(X)$ approach predicted the conversion of particles of various sizes well at temperatures different to that at which the function was derived, thus indicating that the $f(X)$ solely dependent on the evolution of the morphology of the particle.

Keywords

Calcium looping; Modelling; Calcination; Pore evolution;

List of symbols

A_A, A_K, A_C	Coefficients in pressure gradient equation	Pa s m $g^{-0.5}$ $mol^{-0.5}$
$A_{s,0}$	Initial pore area per unit mass	m^2 g^{-1}
$C_{p,n}$	Molar heat capacity of species *n*	J mol^{-1} K^{-1}
$D_{A,nm}$	Diffusivity at arbitrary Knudsen number, for species *n* and *m*	m^2 s^{-1}
$D_{B,nm}$	Molecular diffusivity, involving species *n* in *m*	m^2 s^{-1}
$D_{K,n}$	Knudsen diffusivity of species *n*	m^2 s^{-1}
D_{ref}	Molecular diffusivity $D_{B,12}$ at bulk condition	m^2 s^{-1}
$\overline{d_b}$	Mean bubble diameter	m
E_a	Activation energy	kJ mol^{-1}
H_n	Partial molar enthalpy of species *n*	J mol^{-1}
H_f	Partial molar enthalpy of formation	J mol^{-1}
h	Bed height	m
h_{mf}	Bed height at minimum fluidisation	m
J_n	Total molar flux of species *n*	mol m^{-2} s^{-1}
k_c	Rate constants of calcination reaction	mol m^{-2} s^{-1}
k_c'	Modified rate constants of calcination reaction	s^{-1}
k_0	Arrhenius coefficient of rate constant k_c'	s^{-1}
$\bar{k}$	Rate constant of carbonation reaction	m s^{-1}
M_n	Molecular mass of species *n*	g mol^{-1}
P	Total pressure	bar
P_{bulk}	Bulk pressure	bar
$p_{\mathrm{CO_2}}\|_r$	Local partial pressure of CO_2	bar
$p_{\mathrm{CO_2}}^{\mathrm{bulk}}, p_{\mathrm{CO_2}}^{eq}$	Bulk and equilibrium partial pressure of CO_2	bar
q_{c}	Intrinsic rate of calcination per unit of surface area	mol m^{-2} s^{-1}
Q_n	Net rate of change of species *n* inside the particle	mol m^{-3} s^{-1}
r	Radial distance from the particle centre	m
r_p	Radius of a limestone particle	m
r_{pore}	Mean radius of the pore	nm
R	Universal gas constant	kJ mol^{-1} K^{-1}
t	Time	s
T	Absolute temperature	K
T_{bulk}	Bulk temperature	K
U_b	Bubble velocity	m s^{-1}
U_{mf}	Flow velocity at minimum fluidisation	m s^{-1}
u_M	Mass-averaged velocity	m s^{-1}
$V_{M,\mathrm{CaO}}$	Molar volume of CaO	m^3 mol^{-1}
$V_{M,\mathrm{CaCO_3}}$	Molar volume of $CaCO_3$	m^3 mol^{-1}
X	Solid conversion	-
y_n	Mole fraction of species *n*	-
Greek letters		
Λ_{k_c}	Pre-exponential coefficient of the rate constant k_c	mol m^{-2} s^{-1}
λ_{eff}	Effective thermal conductivity of the particle	W m^{-1} K^{-1}
ε_0	Initial porosity of the particle	-
ε_b	Bubble fraction	-
ε_{bed}	Porosity of the fluidised bed around the particle	-
$\varepsilon(X)$	Porosity of the particle as a function of conversion	-
ρ_e	Bulk density of a particle	kg m^{-3}
ρ_m	Skeletal density of the particle	kg m^{-3}
τ^2	Tortuosity factor of the particle	-

τ_{bed}^2	Tortuosity factor of the fluidised bed	-
δ	External diffusion boundary layer thickness	m
η_r	Dimensionless radius	-
v_{mix}	Kinematic viscosity of gas mixture	$m^2\ s^{-1}$
v_n	Stoichiometric coefficient of species *n*	-
Subscripts		
n=1, 2	CO_2 and N_2	
Abbreviation		
BET	Brunauer–Emmett–Teller	
CPIM	cylindrical pore interpolation model	
DGM	dusty gas model	
MPTM	mean pore transport model	
OCFE	orthogonal collocation on finite element	
RPM	random pore model	

1 Introduction

Broadly-speaking, two classes of model exist to describe the non-catalytic reaction between a gas and a solid, namely the Shrinking Core Model (SCM) and the Continuous Reaction Model (CRM). The SCM has been commonly used to describe, for example, the calcination of non-porous, virgin particles of limestone (generally close to pure $CaCO_3$), where the reaction occurs at a sharp front which recedes towards the centre of the particle [1]. Generally, the rate of reaction might be limited variously by (i) chemical kinetics, (ii) diffusion through the porous product layer, (iii) transport of heat to or from a reaction interface, or (iv) diffusion through the external gas film. On the other hand, the CRM is a better description where there is slow reaction of a gas, and, or, transfer of heat, within a porous solid across a broad front or the entire particle [1]. **Fig. 1** shows the difference in local conversion profiles between two models at fixed average conversion of particle. The calcination of cycled, as opposed to virgin, limestone, possesses the characteristics of the CRM, where the initially-porous particles, containing a mixture of $CaCO_3$ and unreacted CaO, become more porous as the $CaCO_3$ is calcined to CaO during thermal decomposition. Such particles are created when raw limestone particles have been subjected to a history of cycling between the calcined and carbonated states. This typically would occur when using such Ca-based materials for removing CO_2 from the flue gas of plants such as a power station, cement plant and steel factory in certain schemes for carbon capture and storage. The present work is concerned with these cycled particles.

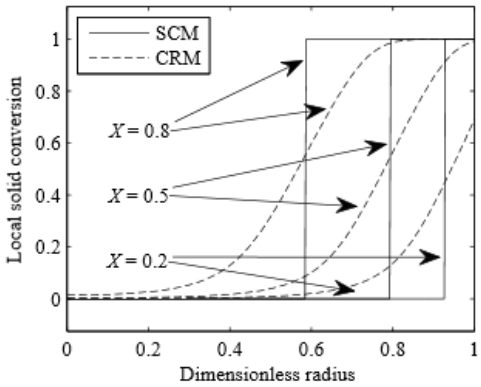

Fig. 1. Local conversion profiles of shrinking core model (SCM) and continuous reaction model (CRM) for fixed average conversion of particle.

A feature of most models of non-catalytic reactions between gases and solids generally is that the intrinsic rate of reaction, r, at a local point within a solid particle is of the form $r = g(C_i, T, P) \times f(X)$ [2,3]. Here, g describes the intrinsic reaction kinetics as a function of the temperature, T, the total pressure, P, and the concentration, C_i, of the reaction gases. The term $f(X)$ is a direct function of the conversion of the particle and is correlated with the internal morphology of the particle, *e.g.* surface area, pore size, pore size distribution *etc*. at a particular conversion. In addition, $f(X)$ is not a function of C_i, T, or P.

Many researchers have sought to model the development of internal pore structure with conversion during non-catalytic gas-solid reaction. For example, Szekely & Evans [4] assumed that solid particles consisted of an array of spherical grains with the space between them making up the voids. They made the first attempt to incorporate the structural parameters such as grain size, porosity and pore size into the reaction scheme in their grain model. Their original model assumed that the pore structure was unaffected by the progress of reaction, although later variants [5] were able to account for change in grain size with reaction. More recently, Liu *et al.* [6] developed an overlapping grain model using a fitted size distribution of grains to account for the evolution of pore structures during reaction. On the other hand, random pore models have been developed, *e.g.* Bhatia & Perlmutter [3] and Gavalas [7], using different approaches based on cylindrical pore assumptions, to model the total surface area at any conversion as a function of the initial morphological parameters, *e.g.* the initial porosity. In a somewhat different approach, Simons & Finson [8] built a mass transport model using statistical methods to specify the pore structure as a continuously branching tree. However, in his model the small pore trees will be kinetically limited while the larger pore trees are diffusion limited. This is the opposite of one might expect for pores with uniform length. The existing mathematical pore models such as the random pore model, statistical pore tree model and grain model contain parameters that are difficult to measure and thus become fitting parameters, *e.g.* the diffusivity of SO_2 through a layer of $CaSO_4$, which are complicated and equally arbitrary. In many cases, the use of mathematical pore models leads to the need to modify the original models in order to fit experimental measurements [9–11].

On the other hand, the experimentally-determined $f(X)$ function from the common measurements of reaction rate and conversion offers a straightforward method to describe the change of internal morphology at a local point within the particle being reacted under conditions affected by intraparticle mass transfer [12]. This is exemplified by recent studies of char gasification in a fluidised bed [12,13], where it was found that a simple, arbitrary function, $f(X)$, could be determined from the plot of measurements of rate *vs.* conversion of the solid char in the kinetically-controlled regime. It was proposed that the ratio between the rate of reaction at any conversion and the initial rate of reaction reflects, generally, the variation in the pore structure as the reaction proceeds in the absence of intraparticle mass transfer limitation (*e.g.* at low temperature or using small particles or with particles of low reactivity) [13], thus giving $f(X) = r(X)/r(X = 0)$.

Dai *et al.* [12] concluded that the application of the $f(X)$ concept to the gasification of chars by CO_2 suffered the complication of there being multiple types of active sites for adsorption on the surface of char so that a single $f(X)$ determined from experimental measurements at a low temperature was unable to fit satisfactorily all the measurements made at a substantially higher temperature. Accordingly, to investigate the basic hypothesis that

a gas-solid reaction can be characterised by $r = g(C_i, T, P) \times f(X)$, it is important to identify a solid which is unlikely to contain sites which vary in relative activity with temperature. The conversion of calcium carbonate to calcium oxide does not involve gas adsorption, thus limestones is a potential suitable candidate. Of course, as noted above, virgin limestone ($CaCO_3$) is almost non-porous, and the calcination reaction usually follows a shrinking core mechanism [14,15], unsuitable for the application of the $f(X)$ concept. However, limestones which have been successively calcined to CaO and carbonated in CO_2 back to $CaCO_3$ many times, present a different type of porous solid, which can be described by a CRM, as noted above. This is because the recarbonation is never complete and so after many cycles, the starting, carbonated material is, in fact, quite porous and so provides an appropriate candidate for verifying the $f(X)$ hypothesis. The purpose of this paper is therefore to examine if the $f(X)$ concept can be used for modelling non-catalytic gas – solid reactions, other than those involving gasification, using calcination as an example for different particle sizes and over a range of temperatures.

2 Experimental

2.1 Materials

Table 1. Composition of the fresh limestones in wt%.

Component	Ca	Fe	Mg	Ni	Al	K	Mn	Si	S	Zr	Sr	Ti
Compostilla	89.70	2.50	0.76	0	0.16	0.46	0	0.07	0	0	0	0.37
Purbeck	97.67	0.49	0.61	0	0.21	0.09	0.14	0.65	0.11	0.05	0	0

The gases used in the experiments were N_2 ($\geq$ 99.9 vol%, oxygen $\leq$ 2 ppmv) and CO_2 ($\geq$ 99.8 vol%). All gas cylinders were supplied by BOC or Air Liquide. Natural, uncrushed silica sand (fraction C, David Ball Group plc., dry), sieved to 355 – 425 μm, was used as a fluidised bed material. The density of the non-porous sand particles was ~ 2690 kg m^{-3}. Two types of limestone particles were used: (i) a Spanish limestone (Compostilla) after 8 cycles of calcination and carbonation, and (ii) a British limestone (Purbeck) after 6 such cycles. The number of cycles was chosen so that the particles become porous and the ultimate CO_2 uptake by the limestones of the current cycle was close to that of the previous cycle. The compositions of the fresh limestones are shown in **Table 1**. After cycling, the internal pores of the limestone, even at the start in the fully-carbonated state, were macro-pores (> 50nm) so that the calcination would likely occur continuously throughout the entire particle, as shown in **Table 2**. The cycling of the limestone particles was conducted in a bed of sand fluidised by 15 vol% CO_2 balance N_2 at 1 atm. The limestone particles were calcined at 1173 K for 10 minutes and then carbonated at 923 K for 10 minutes. Here, the temperature at which a partial pressure of CO_2 of 0.15 atm is in thermodynamic

equilibrium with a mixture of CaO and $CaCO_3$ was calculated to be 1053 K [16]. The resulting carbonated particles were cooled in a desiccator and then were sieved from the sand. Two sieve size fractions were used in the experiments for each type of limestone: 710 – 850 μm and 1400 – 1700 μm. These sizes were selected in order to recover the cycled particles effectively from the sand and to compare the theoretical predications across different particle size.

2.2 Fluidised bed experiments

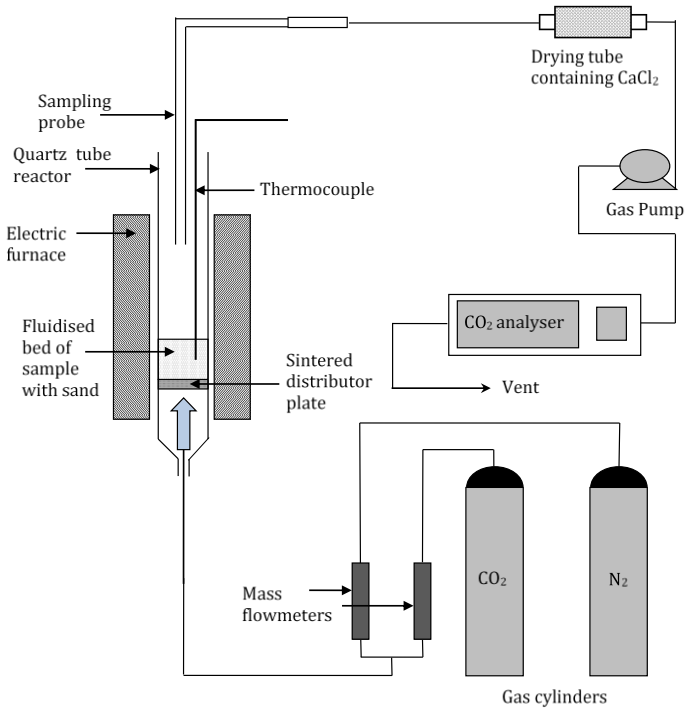

Fig. 2. Schematic diagram of the arrangement for batch experiments in a quartz reactor (i.d. 30 mm).

Batch experiments were performed in a fluidised bed contained in a quartz reactor, internal diameter 30 mm and length 460 mm, provided with a porous frit (4 mm thick, pore size 100 – 160 μm) as the distributor, situated 110 mm from the base of the reactor. By using pressure taps at the inlet and the outlet, the pressure drop across the distributor and a 20 ml sand bed was measured to be 13 – 15 mbar at experimental conditions. The reactor was externally heated by an electric furnace. The temperature of the bed was measured by a K-type thermocouple (2 mm dia.) inserted into the top, with its tip 20 mm above the distributor. Flowrates of N_2 were controlled by a mass flow meter calibrated at 293 K and 1 bar. The off-gas leaving the fluidising bed was sampled at 16.7 mL s^{-1} (STP) through a quartz tube. To prevent elutriated particles and water vapour in the sampled gas entering the analysers, the gas was passed through a glass wool filter and a drying tube filled with $CaCl_2$ in series. The mole fractions of CO_2 were measured by a non-dispersive infra-red gas analyser (ABB EL3020). Fig. 1

shows the arrangement of the apparatus. In an experiment, the reactor was filled with 20 ml of silica sand and heated to the desired temperature, *viz.* 1023 – 1173 K. For calcination, the fluidising gas was 100 mol% N_2. The total volumetric flowrate was 80 mL s^{-1} (STP), giving $U/U_{mf} \sim 6.3 – 7.9$, with U being the superficial velocity at the temperature of the bed and U_{mf} being the value at incipient fluidisation predicted from the correlation of Wen and Yu [17]. From experimental measurements using different sample masses ranging from 0.1 – 0.5 g at 1173 K, the measurement of reaction rate starts decreased when the sample mass was bigger than 0.3 g due to complications arising from mass transfer between the bubble and the particulate phases. Hence a sample mass of 0.3 g was chose for all experiments. Each experiment was repeated at least 3 times. To ensure complete calcination of the limestones, the calcination experiment is ended 10 seconds after the measured concentration of CO_2 of the off-gas returns to zero.

2.3 Characterisation of the limestone particles

Table 2. Particle characterisation of fully carbonated limestones.

Limestone	BET analysis			Mercury intrusion porosimetry					
	BET area / m^2 g^{-1}	BJH volume / cm^3 g^{-1}	BJH adsorption mean pore diameter / nm	Porosity	Total pore area / m^2 g^{-1}	Total intrusion volume / cm^3 g^{-1}	Mean pore diameter / nm	Bulk density / kg m^{-3}	Tortuosity factor / -
Compostilla, 8 cycles	0.33	7.2×10^{-3}	72	0.16	0.46	0.070	608	2235	2.8
Purbeck, 6 cycles	1.58	9.9×10^{-3}	21	0.34	3.88	0.188	190	1811	2.1

Table 2 shows the measurements from the Brunauer–Emmett–Teller (BET) analysis (TriStar 3000) and mercury intrusion porosimetry (AutoPore IV 9500), both of which produce a pore size distribution of the particles. It is clear that these cycled particles have substantial pore volume, even in their fully-carbonated state, in contrast to virgin limestone, which has negligible porosity. In the subsequent modelling, the mean pore diameter $d_{pore} = 4V/A$ from mercury porosimetry was used as the initial pore diameter of the particles, where V is the total intrusion volume and A is the total pore area. It should be noted that the limestone particles may have considerable unmeasured surface area and pore volume in the micro-porous range ($d_{pore} < 2$ nm), as the BET and mercury intrusion analyser were unable to measure pore diameters smaller than 1.7 nm and 3 nm respectively.

Dai *et al.* [12] measured the particle size distribution of 600 – 1000 μm dia. char particles with the same sub-angular shape to the limestone particles by optical microscopy and showed that the effective particle diameter

$D(3,2) \times \psi$, where $D(3,2)$ was the Sauter mean diameter and ψ is a shape factor, is very close to the geometric mean of the mesh sizes. Therefore in the model, the mean, external particle diameter d_p was calculated from the geometric mean of the sieves d_p = (lower mesh × upper mesh)$^{0.5}$.

3 Theoretical

The model described in this work assumed that the limestone particle is spherical and is calcined in a bed of silica sand fluidised by a stream of N_2. The only reaction occurring is:

$$CaCO_{3(s)} \rightleftharpoons CaO_{(s)} + CO_{2(g)} \qquad \Delta H^0_{298K} = +178 \text{ kJ mol}^{-1} \qquad \text{(I)}$$

The two principal assumptions were:

i) The material and energy balances inside and outside the particle are in pseudo-steady state, so that the gas concentrations, total fluxes, total pressure and temperature have no time dependence. By using the pseudo-steady state assumption here, it means that the time needed to establish an initial steady concentration profile is very small. Without this assumption, the initial concentration would have been zero everywhere. Nevertheless, as justified by Bischoff [18], the profiles generated using this assumption will be achieved very quickly in a gas-solid system. In fact, the thermal diffusivity of the solid at 800 °C is about 9×10^{-6} m^2/s, even for a 2 mm dia. particle, the time constant estimated from Radius^2 / (2 × thermal diffusivity) is very small ~ 0.2 s. Wen [19] also concluded that the pseudo-steady state solution was a good approximation for most of the solid-gas reaction systems except for systems with extremely high pressure and very low solid reactant concentration. However, the balances are affected indirectly by the conversion X which does have time dependence and affects the physical properties of the particle (*e.g.* porosity, pore diameter and particle size).

ii) The evolution of the internal morphology of a limestone particle during calcination can be described by an arbitrary $f(X)$, a function of X – the local conversion of the maximum available $CaCO_3$ content within the particle after cycling. The reason for such a definition of conversion is that the limestone particle is only partially carbonated and the maximum CO_2 uptake decays gradually with the number of cycles. Hence the reaction rate at some point within the solid can be expressed in the form of $r = g(C_i, T, P) \times f(X)$. It was assumed that $f(X)$ applies everywhere within a particle and is independent of temperature. The value of $f(X)$ changes with the local conversion, which will vary with distance from the centre of the particle. The $f(X)$ can be obtained from a plot of the experimental rate of calcination against conversion obtained from experimental measurements in which the rate is controlled *solely* by intrinsic chemical kinetics [12,13].

3.1 The kinetics of the calcination reaction

The intrinsic rate of reaction per unit of surface area for reaction (I) was given by [14]

$$-q_c = k_c - \bar{k} C_{CO_2} = k_c - \bar{k}\, p_{CO_2}/RT \quad (1)$$

where k_c is the rate constant of the calcination reaction (here, in mol m^{-2} s^{-1}), $\bar{k}$ is the rate constant of the reverse, carbonation reaction (m s^{-1}) and p_{CO_2} is the partial pressure of CO_2. At equilibrium, the rate $q_c = 0$, so that $k_c - \bar{k}\, p_{CO_2}^{eq}/RT = 0$. Therefore, the ratio of rate constants is:

$$k_c/\bar{k} = p_{CO_2}^{eq}/RT \quad (2)$$

Substituting Eq. (2) into Eq. (1),

$$-q_c = k_c\left(1 - p_{CO_2}/p_{CO_2}^{eq}\right) \quad (3)$$

Here $p_{CO_2}^{eq}$ is the equilibrium partial pressure of CO_2 at local conditions. Barin and Platzki [16] gave the following expression for $p_{CO_2}^{eq}$:

$$p_{CO_2}^{eq} = 4.083 \times 10^7 \exp(-20474/T) \quad (4)$$

where the unit of T is in K. The rate constant k_c was assumed to be an activated quantity, thus $k_c = \Lambda_{k_c} \exp\left(-E_a/RT\right)$.

Based on the assumption ii), the rate of reaction per unit volume of particle, Q_C, is:

$$Q_C = q_c A_{s,0} \rho_{e,0} f(X) = -k_c\left(1 - p_{CO_2}/p_{CO_2}^{eq}\right) A_{s,0} \rho_{e,0} f(X) \quad (5)$$

where the parameter $A_{s,0}$ is the initial pore area per unit mass and $\rho_{e,0}$ is the initial bulk density of the particles.

3.2 Equations of mass balance

A pseudo-steady mass balance over a spherical shell at radius r gives the flux equations for CO_2 and N_2:

$$\frac{1}{r^2}\frac{d}{dr}(r^2 J_n) = Q_n = -\nu_n Q_C = -\nu_n q_c A_{s,0} \rho_e f(X) \qquad n = 1, 2 \quad (6)$$

where J_n is the total flux (*i.e.* diffusive flux + advective flux) of species n. The parameter Q_n is the net rate of reaction of species n, in mol m^{-3} s^{-1}, which is positive for a net gain and negative for a net loss in species, and ν_n is the stoichiometric coefficient of species n in reaction (I). The subscripts 1 and 2 are used to represent CO_2 and N_2. A material balance on carbon across a differential element gives the variation of local conversion of $CaCO_3$ with respect to time:

$$\left.\frac{dX}{dt}\right|_r = -M_{CaCO_3}\left(\frac{Q_C}{\rho_{e,0}}\right) = k_c A_{s,0} M_{CaCO_3}\left(1 - p_{CO_2}/p_{CO_2}^{eq}\right) f(X) \quad (7)$$

the initial condition of which is:

$$t = 0: \quad X(r) = 0 \quad \text{for all } r \in [0, r_p] \tag{8}$$

where the particle centre is $r = 0$ and the particle surface is $r = r_p$. Since $A_{s,0}M_{\mathrm{CaCO_3}}$ is the initial pore area per unit volume of particle – a constant, the product of parameters $k_c A_{s,0} M_{\mathrm{CaCO_3}}$ can be replaced by a modified rate constant k_c':

$$\left.\frac{dX}{dt}\right|_r = k_c'\left(1 - p_{\mathrm{CO_2}}/p_{\mathrm{CO_2}}^{eq}\right) f(X)$$
$$k_c' = \Lambda_{k_c} A_{s,0} M_{\mathrm{CaCO_3}} \exp(-E_a/RT) = k_0 \exp(-E_a/RT) \tag{9}$$

The activation energy of k_c' is the same as that of k_c, but the pre-exponential becomes $k_0 = \Lambda_{k_c} A_{s,0} M_{\mathrm{CaCO_3}}$.

3.3 Equations of intraparticle mass transfer

A model of multi-component diffusion based on the Stefan-Maxwell equations within a porous medium was needed to describe the intraparticle diffusion rigorously. The two principal flux models for non-equimolar, multi-component mass transfer are the Dusty Gas Model (DGM) [20], and the Mean Pore Transport Model (MPTM) [21–23]. Given that both models are algebraically complicated, Young and Todd [24] developed a new MPTM called the Cylindrical Pore Interpolation Model (CPIM). Comparing all three models, the CPIM has a more rigorous treatment of continuum flow, a clearer interpolation procedure for transitional flow and a more compact form of the working equations which helps to clarify the roles of the governing parameters. Recent studies suggest that the CPIM is well suited to modelling multi-component diffusion in both catalyst pellets [25] and in gasifying char particles [12,13]. For this reason, the CPIM was selected to model intraparticle diffusion in the present work. The governing equations are:

$$\frac{dy_n}{dr} = \frac{\tau^2 RT}{\varepsilon P} \sum_{m=1}^{2} \left(\frac{y_n J_m}{D_{A,mn}} - \frac{y_m J_n}{D_{A,nm}} \right) \qquad n = 1, 2 \tag{10}$$

$$\frac{dP}{dr} = -\frac{\tau^2 A_A}{\varepsilon} \sum_{n=1}^{2} \left(\sqrt{M_n} \cdot J_n \right) \tag{11}$$

The boundary conditions for the above equations are given at the centre ($r = 0$) and the surface ($r = r_p$) of the particle:

$$r = 0: \quad J_1 = 0 \quad J_2 = 0 \tag{12}$$

$$r = r_p: \quad y_n = y_n^{\text{surface}} \quad (n = 1, 2) \quad \& \quad P = P_{\text{surface}} \tag{13}$$

Here, y_n is the mole fraction of species n, τ^2 represents the tortuosity factor of the particle from mercury intrusion porosimetry measurements, ε is the porosity at the local point, which varies with conversion and is discussed later,

and M_n is the molar mass of gas species n. The parameters $D_{A,nm}$ and A_A were found by interpolating between the extremes of continuum and Knudsen flow using the equations proposed by Young and Todd [24]:

$$\frac{1}{D_{A,nm}} = \frac{1}{D_{K,n}} + \frac{1}{D_{B,nm}} \qquad \frac{1}{A_A} = \frac{1}{A_K} + \frac{1}{A_C} \tag{14}$$

where $D_{B,nm}$ is the molecular diffusivity calculated from the Chapman-Engskog theory using the Lennard-Jones (6-12) potential [26]. The error in the predicted binary diffusivities by this method is ~ 7.3% [27]. $D_{K,n}$ is the Knudsen diffusivity and the parameters A_K and A_C are the coefficients in the pressure gradient equation in the continuum and Knudsen regime, given by [24,28]

$$D_{K,n} = \frac{2r_{pore}}{3}\sqrt{\frac{8RT}{\pi M_n}} \qquad A_K = \frac{3}{4r_{pore}}\sqrt{\frac{\pi RT}{2}}$$
$$A_C = 8\mu_{mix}RT \Big/ \left(Pr_{pore}^2 \sum_{n=1}^{2} \left(y_n \sqrt{M_n}\right) \right) \tag{15}$$

where the viscosity of the gas mixture, μ_{mix}, was calculated using Chapman-Engskog theory.

The porosity, ε, changes with the local conversion of $CaCO_3$, X, during reaction and can be derived from the volume balance equation for a thin cylindrical shell inside the particle:

$$\varepsilon(X) = \varepsilon_0 + X(1-\varepsilon_0)\left(1 - V_{m,\mathrm{CaO}}/V_{m,\mathrm{CaCO_3}}\right) \tag{16}$$

where $V_{m,\mathrm{CaO}}$ and $V_{m,\mathrm{CaCO_3}}$ are the molar volume of the non-porous CaO and $CaCO_3$ solids. In terms of the pore diameter, it was assumed that the particle has uniform cylindrical pores of initial diameter $d_{pore,0}$; the corresponding initial porosity of the particle was ε_0. Ignoring the small volume of crossing between pore channels, the local porosity can be estimated from $\varepsilon(r) \cdot \delta V = \pi d_{pore}^2 \sum_{i=1} L_i/4$, where δV is the volume of a differential element between r and $r+dr$ and $\sum_{i=1} L_i$ is the sum of the length of the cylindrical pores within the element. Assuming that the evolution of the pores during reaction occurs only in a radial direction so that the pore diameter changes while the length of the pore remains constant, then:

$$\varepsilon(r)/\varepsilon_0 = \left(d_{pore}/d_{pore,0}\right)^2 \tag{17}$$

Substituting Eq. (16) into (17), the pore diameter at some time when the local conversion is X is:

$$r_{pore} = r_{pore,0}\sqrt{\left(\varepsilon_0 + X(1-\varepsilon_0)\left(1 - V_{m,\mathrm{CaO}}/V_{m,\mathrm{CaCO_3}}\right)\right)/\varepsilon_0} \tag{18}$$

3.4 Equations of external mass transfer

The particulate phase of the fluidised bed was considered to have a constant local tortuosity and porosity around the limestone particle. It was also assumed that there is no variation of pressure with radial distance

outside the limestone particle, since the interstitial velocity of fluidising gas – ~1.1 m/s (STP) is much larger than the mass average velocity of gas leaving the surface of a reaction particle – ~0.04 m/s (STP) calculated from the gas flux at the surface. This suggests that there is no tendency to form voids or bubbles around the reacting particle in the case under consideration and that pressure variations outside the particle can be neglected. The general Stefan-Maxwell equations [26] were used to model the external mass transfer within a diffusion boundary layer of thickness δ outside the particle:

$$\frac{dy_n}{dr} = \frac{\tau_{bed}^2 RT}{\varepsilon_{bed} P} \sum_{m=1}^{2} \left(\frac{y_n J_m - y_m J_n}{D_{B,nm}} \right) \qquad n = 1,2 \qquad dP/dr = 0 \tag{19}$$

Here τ_{bed}^2 is the tortuosity factor of the sand bed. It was experimentally measured to be $1.34^2 = 1.80$ for a packed bed with 200 µm dia. quartz sand by Zoia and Latrille [29]. Also, ε_{bed} is the porosity of the bed, assumed to be 0.44, the same as the porosity at incipient fluidisation used by Hayhurst and Parmar [30] for a bubbling fluidised bed of silica sand. The parameter $D_{B,ab}$ refers to the binary molecular diffusivity of species *n* and species *m*. The boundary conditions at the particle surface ($r = r_p$) and the edge of boundary layer ($r = r_p + \delta$) are:

$$r = r_p: \quad J_1 = J_1^{\text{bulk}} \tag{20}$$

$$r = r_p + \delta: \quad y_n = y_n^{\text{bulk}} \quad (n = 1,2) \quad \& \quad P = P_{\text{bulk}} \tag{21}$$

3.5 Equations of energy balance

Outside the limestone particle, convective heat transfer in a bubbling fluidised bed involves packets of sand particles coming into contact with the limestone for a short time, then quickly moving away to be replaced by other packets. It was assumed that the heat transfer coefficient between the particulate phase of the fluidised bed and the surface of the particle was large, so that the particle surface is close to the temperature of the bulk. It was also assumed that the radiative contribution and transpiration contributions to heat transfer were small.

Inside the limestone particle, the energy flux, *E*, is given by [26]

$$E = \sum_{n=1}^{2} M_n J_n \left(\frac{u_M^2}{2} + \frac{H_n}{M_n} \right) - \lambda_{eff} \frac{dT}{dr} \tag{22}$$

Jackson [31] showed that the energy balance can be expressed as $\text{div}(E) = 0$:

$$\frac{1}{r^2}\frac{d}{dr}\left(r^2\frac{dT}{dr}\right)=\frac{1}{\lambda_{eff}}\sum_{n=1}^{2}\left(H_n+\frac{u_M^2}{2}M_n\right)Q_n+\frac{1}{\lambda_{eff}}\frac{dT}{dr}\sum_{n=1}^{2}J_nC_{p,n}$$
$$+\frac{1}{\lambda_{eff}}\sum_{n=1}^{2}M_nJ_nu_M\frac{du_M}{dr} \quad (23)$$

where $C_{p,n}$ is the molar heat capacity of species *n* and λ_{eff} is the effective thermal conductivity. H_n is the partial molar enthalpy of species *n* at temperature *T*, and is calculated from standard enthalpy of formation $H_{f,n}^0$ by $H_n = H_{f,n}^0 + \int_{298}^{T} C_{p,n}dT$. This equation makes specific allowance for the small change in momentum occurring as a result of the change in mass in the gas phase during the non-catalytic decomposition of the solid. The calculation of the thermal parameters C_p and λ is discussed in the next section. Finally, u_M is the mass-averaged velocity of the mixture which is given by $u_M = \sum_{n=1}^{2} M_nJ_n / \sum_{n=1}^{2}\rho_n$. The boundary conditions for the internal energy balance were:

$$r = 0: \quad dT/dr = 0 \qquad r = r_p: \quad T = T_{\text{bulk}} \quad (24)$$

3.6 Calculation of parameters

The initial pore area per unit mass $A_{s,0}$ was obtained from the BET area measurement of the limestone particles. The initial bulk density $\rho_{e,0}$, the initial pore diameter $d_{pore,0}$, the tortuosity factor τ^2 and the initial porosity of the particle ε_0 were determined from the mercury porosimetry measurements, as shown in **Table 2**. Alvarez *et al.* [32] did reported up to 50% increase in pore diameter of natural limestone particles after 100 cycles. In terms of the particle size, Wu *et al.* [33] reported only 2 – 7 % reduction of particle diameter after 10 calcination – carbonation cycles. Hence in this study the overall particle size was assumed to be constant during calcination. Any change of the solid volume due to the difference in molar volumes of $CaCO_3$ and CaO was taken only to affect the pore structure parameters *e.g.* porosity and pore diameter.

The boundary layer thickness δ was given by Hayhurst and Parmar [30]:

$$\text{Sh}_{\text{EMCD}} = 2\varepsilon_{mf}(1 + r_p/\delta) \quad (25)$$

$$\text{Sh}_{\text{EMCD}} = 2\varepsilon_{mf} + 0.61\left(2r_pU_p/\upsilon_{mix}\right)^{0.48}\left(\upsilon_{mix}/D_{B,12}\right)^{0.33} \quad (26)$$

$$U_p = U_{mf}(1-\varepsilon_b)\{1 - 0.5\pi\text{Ln}(1 - 6\varepsilon_b/\pi)\} \quad (27)$$

where $\varepsilon_{mf} = 0.44$ was the voidage at incipient fluidisation for a bubbling fluidised bed with silica sand used by Hayhurst and Parmar [30]. Also, υ_{mix} is the kinematic viscosity of the gas mixture calculated using Chapman-Engskog theory and $D_{B,12}$ the binary molecular diffusivity for CO_2 and N_2. The bubble fraction ε_b was given by

$\varepsilon_b = (U - U_{mf})/U_b = (h - h_{mf})/h$, where $U_b = (U - U_{mf}) + 0.71(g\overline{d_b})^{0.5}$ [34]. Here, h_{mf} was the bed height at incipient fluidisation, measured to be 0.029 m and $\overline{d_b}$ was the mean bubble diameter estimated from the correlation of Darton *et al.* [35]: $\overline{d_b} = 0.54(U - U_{mf})^{0.4} h^{0.8}/(2g^{0.2})$ with h being the expanded height of the bed when fluidised at superficial velocity U. Although the correlation was based on equimolar counter-diffusion (EMCD), it has been shown that it will yield the correct value of δ from Eq. (25), even for non-EMCD [36].

The thermal conductivities of the gases were calculated from $\lambda = C_1 T^{C_2}/(1 + C_3/T + C_4/T^2)$, where $C_1 - C_4$ are constants [27]. The effective thermal conductivity of the particle was calculated from $\lambda_{eff} = (1 - \varepsilon)\lambda_{solid} + \varepsilon\lambda_{gases}$, where $\lambda_{gases} = \sum_1^{a=3} y_a \lambda_a$. The overall thermal conductivity was largely influenced by that of the solid. The reported thermal conductivity of limestone ($CaCO_3$) and lime (CaO) is 2.25 and 0.84 W m^{-1} K^{-1} respectively [27]. The exact mole fraction of $CaCO_3$ and CaO within the particles after cycling was unknown, hence, λ_{solid} was taken to be 1.5 W m^{-1} K^{-1}. The specific heat capacity of each gas was estimated from $C_p = E_1 + E_2 T + E_3/T^2$, where $E_1 - E_3$ are constants from Green and Perry [27].

3.7 Numerical solution

The system is described by Eq. (6) to (24). Both the intraparticle and external mass transfer models have five 1st order ordinary differential equations (ODEs) in the space domain, and hence five boundary conditions are provided. The ODE for conversion is 1st order in the time domain, hence only one initial condition is required. The energy equation is a 2nd order ODE, hence two boundary conditions are required for both the internal and external cases.

The main difficulty in solving the system lies in efficient solution of the large system of equations. A numerical algorithm, Orthogonal Collocation on Finite Elements (OCFE) [37] was written in MATLAB to solve the model. Pseudo-steady state was assumed for all the other variables except for the conversion X. Using the initial condition in Eq. (8), the 1st order time-dependent ODE of local conversion X, Eq. (7), was solved. The value of $X(\eta_r)$ at time $t + \Delta t$ could be calculated based on $X(\eta_r)$ and dX/dt at time t. The relevant model parameters (*e.g.* porosity and pore diameter) were updated with the new value of $X(\eta_r)$, and then the internal and external models were solved for results at time $t + \Delta t$. The iterative process was stopped when the overall conversion reached unity.

Since the model predicts the distributions of reaction rate and conversion across the radius of a particle, the overall values of rate and conversion need to be obtained from integration across the particle radius. For a

distribution of χ (*e.g.* Q_C and X), its volume averaged value can be calculated from $\bar{\chi} = 3\int_0^1 ({\eta_r}^2 \chi) d\eta_r$, where η_r is the dimensionless radius used inside the particle. The integral was evaluated numerically.

4 Results

Fig. 3 shows the raw measurements of CO_2 mole fraction in the off-gas during the calcination of cycled Compostilla (plot a) and Purbeck limestone particles (plot b) in a bed of silica sand fluidised by pure N_2. The figure suggests that the calcination of Compostilla at 1173 K was completed after ~ 50 s while Purbeck at 1173 K finished calcining after 35 s. The peak concentration of CO_2 from Compostilla was about half that of Purbeck, hence the reactivity of Compostilla was significantly less than that of Purbeck. The equilibrium partial pressure of CO_2 at 1173 K is about 1.087 bar, so the concentration driving force $p_{CO_2}/p_{CO_2}^{eq} < 5\%$. Hence this confirms that the fluidised bed was close to a differential reactor, and it is reasonable to use 0% CO_2 as the bulk concentration in the model.

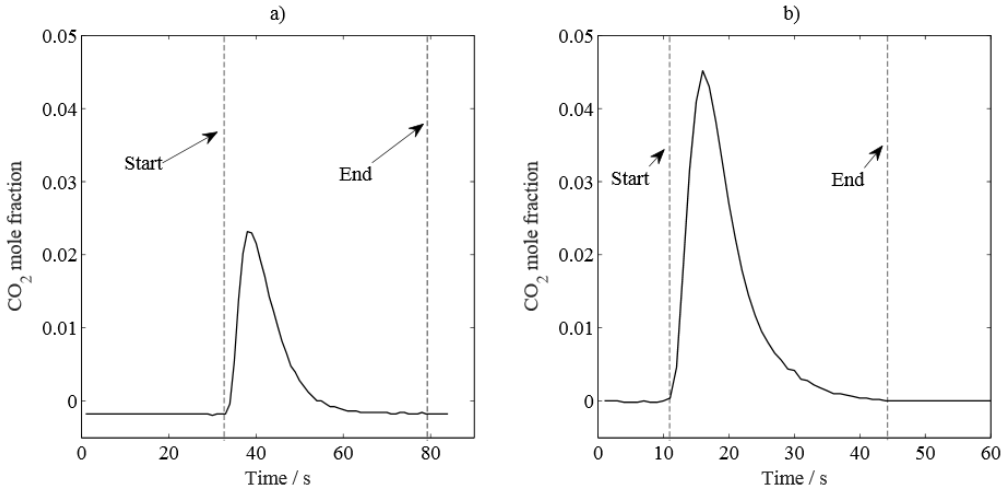

Fig. 3. Measurements of CO_2 mole fraction during calcination of cycled limestones at atmospheric pressure: a) Compostilla 8 cycles 0.71 – 0.85 mm at 1173 K; b) Purbeck 6 cycles 0.71 – 0.85 mm at 1173 K.

The overall rate of production of CO_2 from calcination in s^{-1} is $dX/dt = \left(\dot{N}_{out} y_{CO_2,out} - \dot{N}_{in} y_{CO_2,in}\right) / \int \left(\dot{N}_{out} y_{CO_2,out} - \dot{N}_{in} y_{CO_2,in}\right) dt$. The parameters $\dot{N}_{out}$ and $\dot{N}_{in}$ are the total molar flows leaving and entering the reactor at the exit and entrance conditions, where $\dot{N}_{out}\left(1 - y_{CO_2,out}\right) = \dot{N}_{in}\left(1 - y_{CO_2,in}\right)$ from the mass balance of nitrogen. The raw measurements were deconvoluted to account for the mixing and delay in the sampling line using the method described by Saucedo *et al.* [13].

Table 3. Kinetic parameters of the calcination of 0.71 – 0.85 mm dia. limestone particles.

Limestone particles	k_0 / s^{-1}	E_a / kJ mol^{-1}

Compostilla, 8 cycles	1.72×10^{7}	175 ± 12
Purbeck, 6 cycles	6.50×10^{7}	186 ± 5

The Arrhenius coefficients and activation energies of the kinetic parameter k_c' in Eq. (9), shown in Table 3, were determined from the initial rate extrapolated from the experimental measurements, as shown in **Fig. 4**. At the start of reaction, the particle conversion is 0 and $f(X) = 1$, and Eq. (9) can be rearranged

$$\mathrm{Ln}(dX/dt\,|_{t=0}) = -E_a/RT + \mathrm{Ln}(k_0) + \mathrm{Ln}\left(1 - p_{\mathrm{CO_2}}/p_{\mathrm{CO_2}}^{eq}\right) \quad (28)$$

If the value of $p_{\mathrm{CO_2}}/p_{\mathrm{CO_2}}^{eq}$ is much smaller than 1, which is usually the case if the reaction is controlled by intrinsic kinetics, then

$$\mathrm{Ln}(dX/dt\,|_{t=0}) = \mathrm{Ln}(k_c') = -E_a/RT + \mathrm{Ln}(k_0) \quad (29)$$

A plot of $\mathrm{Ln}(dX/dt\,|_{t=0})$ *vs.* $1/T$ should therefore yield the activation energy E_a and the Arrhenius coefficient k_0. The linearity of **Fig. 5** and **Fig. 8** in section 4.1 and 4.2 respectively show that the calcination of the limestone was indeed controlled by chemical kinetics at low temperature, hence confirming the use of Eq. (29) for the determination of the kinetic parameters. The errors associated with the kinetic parameters mainly come from extrapolating the initial rates from measurements, and using a limited number of measurements for linear regression analysis. The 95% confidence intervals of the kinetic parameters are shown in **Fig. 5** and **Fig. 8**.

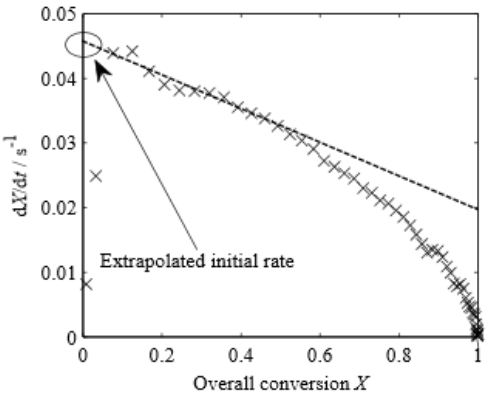

Fig. 4. Determining initial rate of reaction using linear extrapolation (--) on rate and conversion measurements (×) of Compostilla 0.71 – 0.85 mm particles (8 cycles) at 1073 K.

4.1 Calcination of Compostilla limestone particles

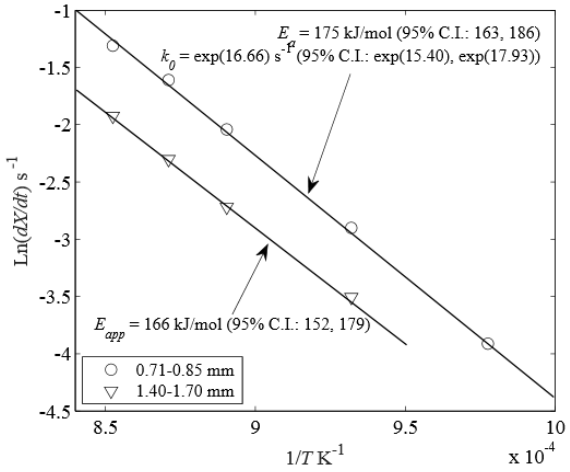

Fig. 5. Determining the kinetic parameters of Compostilla limestone particles (8 cycles). The measurements were obtained from the calcination of the limestone particles at 1023 K (0.71 – 0.85 mm only), 1073 K, 1123 K, 1148 K and 1173 K. The values of the kinetic parameters of the rate constant are shown with 95% confidence interval (C.I.).

Particles of Compostilla limestone with diameters of 0.71 – 0.85 mm and 1.40 – 1.70 mm were calcined at 1023 K (0.71 – 0.85 mm only), 1073 K, 1123 K, 1148 K and 1173 K. Using the initial rate extrapolated to zero conversion, **Fig. 5** shows that the plot of $\mathrm{Ln}(dX/dt)$ *vs.* $1/T$ of each particle forms straight lines. The values of the kinetic parameters in Eq. (9) were determined from a linear regression analysis, yielding an activation energy of $E_a = 175 \pm 12$ kJ/mol and $k_0 = 1.72 \times 10^7$ s^{-1} for 0.71 – 0.85 mm dia. particle. For 1.40 – 1.70 mm dia. particle, the reaction rates were lower than those of 0.71 – 0.85 mm dia. particle and the apparent activation energy was 166 ± 14 kJ/mol, representing a 9 kJ/mol reduction that is within an error band of ± 12 kJ/mol. It is expected that the gradient of a best fit line would approach a half of its intrinsic value if the reaction rate were significantly limited by intraparticle mass transfer [1]. However, this is not observed in **Fig. 5**. The values of the activation energy indicate that the reactions could not have been in mass transfer limited regime. Hence, it can be concluded that (i) the calcination of 0.71 – 0.85 mm dia. particles was controlled by intrinsic chemical kinetics; (ii) the reactions of 1.40 – 1.70 mm dia. particles were possibly affected by intraparticle mass transfer but not severely so.

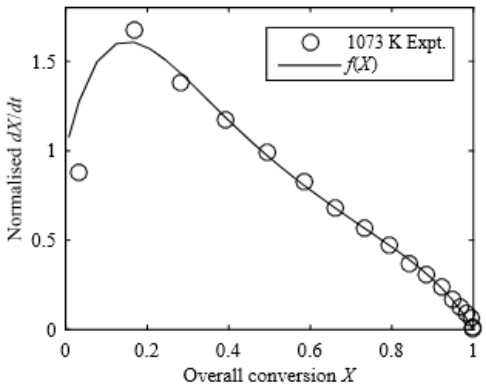

Fig. 6. Determining the function $f(X)$ from the plot of normalised rate *vs.* conversion measurement of 0.71 – 0.85 mm dia. Compostilla (8 cycles) at 1073 K.

The form of $f(X)$ needs to be determined from experimental measurements of calcination rate *vs.* conversion conducted under conditions where the reaction is controlled by intrinsic chemical kinetics. Owing to the low rate of reaction at 1023 K, the percentage fluctuation caused by random noise in the measurements of CO_2 concentration was very large. The resulting $f(X)$ was not a smooth function, as expected. However, since experiments at both 1023 K and 1073 K appear to be in the regime of chemical kinetic control, as shown in **Fig. 5**, the $f(X)$ function was determined from the measurements at 1073 K instead. **Fig. 6** shows the plot of $f(X)$, a 6^{th} order polynomial of X, determined from the normalised rate *vs.* conversion measurements of Compostilla limestone of sieve diameter 0.71 – 0.85 mm, calcined at 1073 K. The figure shows a peak higher than 1 at about 20% conversion. This is due to the fact that part of the surface area that is previously unreachable become accessible when the solid volume reduces during the initial stage of calcination. This increase in surface area only occurs at low conversion when the coalescence of pores is insignificant. Using this $f(X)$, the model was able to fit well the experimental results at 1023 K, as seen in Fig. 7(a). This strongly suggests that the $f(X)$ was not merely a fit valid for one particular experimental condition.

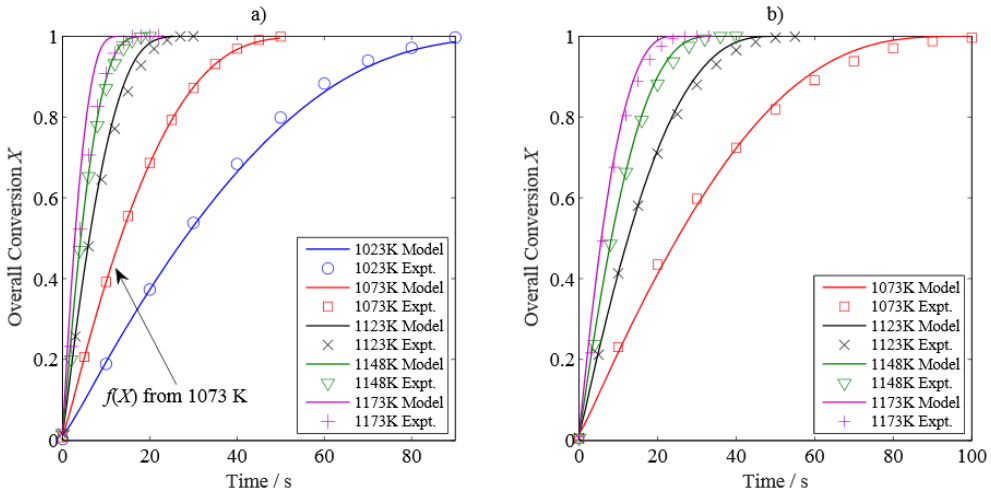

Fig. 7. Comparison of model results (lines) with experimental measurements (points) of the calcination of Compostilla limestone particles (8 cycles) by 100% N_2: a) 0.71 – 0.85 mm; b) 1.40 – 1.70 mm. The $f(X)$ was determined from the rate *vs.* conversion measurements of 0.71 – 0.85 mm particles at 1073 K, and was applied to all cases.

Further comparisons between model predictions and experimental measurements for Compostilla limestone of 0.71 – 0.85 mm dia. and 1.40 – 1.70 mm dia. are shown in **Fig. 7**, with generally good agreement being seen between experiment and theory. However, the experimental measurements for the 0.71 – 0.85 mm dia. particle at 1173 K were almost identical to those at 1148 K, which indicates either a severe limitation by external mass transfer or experimental error arising from the rapidity of the reaction and the problem in correcting for mixing in the sampling line. **Fig. 5** shows that even for the larger particles at higher temperature, the rate of reaction was not limited by mass transfer as the gradients of the two measurements are almost the same. Therefore it can be concluded that the unexpected behaviour of the rate of 0.71 – 0.85 mm dia. at 1173 K is due to error.

4.2 Calcination of Purbeck limestone particles

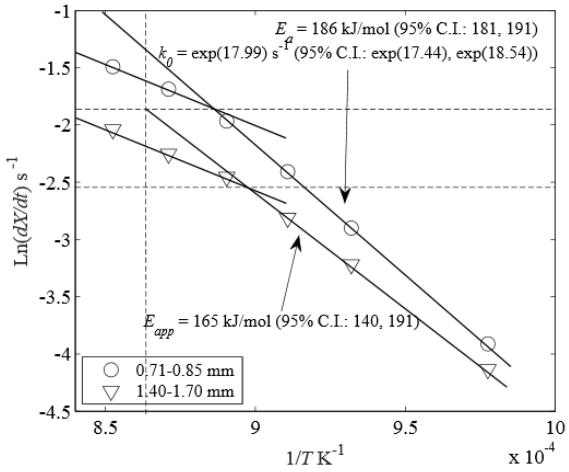

Fig. 8. Determining the kinetic parameters of Purbeck limestone particles (6 cycles). The measurements are from calcination of 0.71 – 0.85 mm and 1.40 – 1.70 mm particles at 1023 K, 1073 K, 1098 K, 1123 K, 1148 K and

1173 K. The gradient of the linear regression line for both particles reduced by ~ 50% at 1098 – 1173 K. The values of the kinetic parameters are shown with 95% confidence interval (C.I.).

Experiments with Purbeck limestone were performed using 0.71 – 0.85 mm and 1.40 – 1.70 mm dia. particles at 1023 K, 1073 K, 1098 K, 1123 K, 1148 K and 1173 K. The same kinetic analysis was performed on the experimental measurements and the results are shown in **Fig. 8**. A linear regression line of the plot of $\mathrm{Ln}(dX/dt)$ *vs.* $1/T$ gives an activation energy $E_a = 186 \pm 5$ kJ/mol and the rate constant $k_0 = 6.50 \times 10^7$ s^{-1}. At 1098 – 1173 K, the gradient of the regression lines of measurements, thus $-E_a/R$, is reduced by about half at $T >$ 1098 K. Hence, this figure suggests that the transition of the reaction regime from chemical kinetic control to mass transfer control starts at ~ 1098 K. **Fig. 8** also shows that the rates of reaction of the 1.40 – 1.70 mm dia. particles are lower than those of the 0.71 – 0.85 mm dia. particles; the linear regression lines of the 1023 – 1098 K measurements show a 21 kJ/mol decline, larger than the ± 5 kJ/mol error, in the apparent activation energy, probably owing to a growing influence of the mass transfer limitation for larger particles. At $T >$ 1098 K, the slope of the points of 1.40 – 1.70 mm dia. particle is almost the same as that of 0.71 – 0.85 mm particle, suggesting that the reaction becomes limited by mass transfer. Furthermore, for the 1.40 – 1.70 mm dia. particles the transition of the reaction regime occurs at a temperature lower than that of the 0.71 – 0.85 mm dia. particle, a consequence of the increased mass transfer limitation in larger particles.

Fig. 9 compares the rates of conversion *vs.* time from experimental measurements (points) with the theory (line) for Purbeck limestone calcined in 100% N_2 at 1023 – 1173 K. Interestingly, the $f(X)$ determined previously from the measurements on Compostilla limestone of 0.71 – 0.85 mm dia. at 1073 K, shown in **Fig. 6**, was successfully applied here for both size fractions of Purbeck limestone. The result shows that the model fits perfectly with the experimental measurements even for measurements at 1173 K.

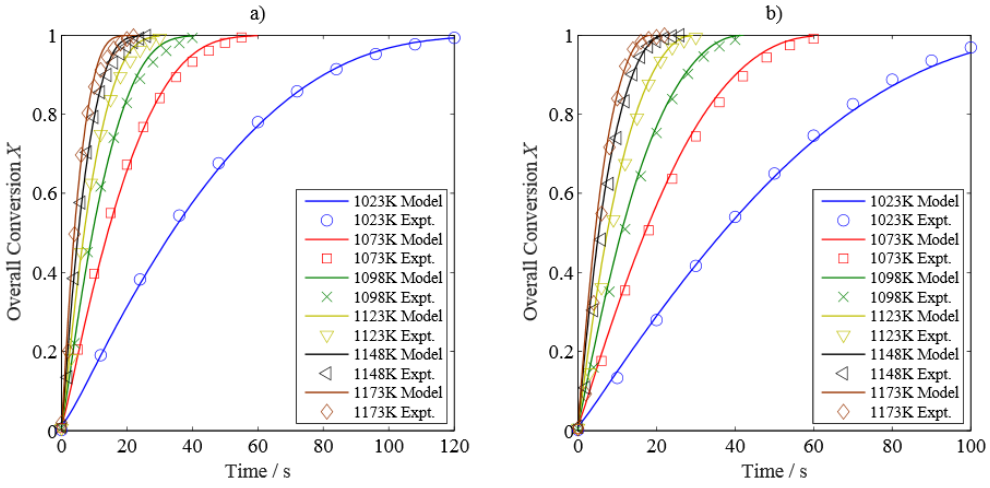

Fig. 9. Comparison of model results (lines) with experimental measurements (points) of the calcination of Purbeck limestone particles (6 cycles) by 100% N_2: a) 0.71 – 0.85 mm; b) 1.40 – 1.70 mm. The $f(X)$ determined from Compostilla 710 – 850 μm particles at 1073 K was used here.

Given the results, it can be concluded that using a constant $f(X)$ across different temperatures gives a satisfactory agreement between the model and the measurements for both Compostilla and Purbeck limestone. The fact that the $f(X)$ obtained from measurements of Compostilla could be successfully applied to the modelling of Purbeck suggests that the two limestone particles experienced similar changes of internal morphology during calcination. One reason that could explain this is that both particles had been periodically cycled several times before the final calcination reaction, which could have reduced the variations in pore structures thus making the two types of limestone particles more similar in terms of internal morphology. In addition, after a number of calcination – carbonation cycles, the reactivity of the particles approaches an asymptotic value. It might also be the case that the internal pore structure had developed into an "asymptotic" stage, where the original variations in pore structures between the two limestones had become slight on cycling.

5 Discussion

The above research is concerned with limestone which has been successively calcined and carbonated several times. Experimentally, the observed activation energies for the calcination of cycled, carbonated material were reasonably close to values in the literature, lying between 160 and 210 kJ/mol [14,15,38–40] for the calcination of virgin limestones, being 175 ± 12 kJ/mol and 186 ± 5 kJ/mol, respectively, for the Compostilla and Purbeck. These values, being close to the standard enthalpy of calcination, +178 kJ/mol, suggest that the activation energy for the reverse, carbonation reaction is small, being ~ -3 kJ/mol for Compostilla and ~ +8 kJ/mol for Purbeck. Thus, the intrinsic rate of carbonation changes little with temperature in the range of the temperature studied in the paper. Zawadzki and Bretsznajder [41] found that the rate of carbonation varies linearly with the difference between the partial pressure of CO_2 and its equilibrium value at 328 – 368ºC, which suggested that the rate constant was the same for all temperature thus a zero activation energy of the carbonation rate. Nitsch [42] also concluded that the rate of carbonation has an activation energy close to zero as the rate versus partial pressure difference gave a single linear line for measurements at 800 – 850ºC. The same conclusions were also reached by Bhatia and Perlmutter [43] and Dennis and Hayhurst [14] for carbonation experiments at 823 – 998 K and 1073 – 1248 K respectively.

Comparing the reaction rates of both limestones in **Fig. 5** and **Fig. 8**, it can be seen that the reactivity of Compostilla is slightly lower than that of Purbeck for 0.71 – 0.85 mm dia. particles. In addition, **Table 2** shows that the mean pore diameter of Purbeck limestones is only ~1/3 of that of Compostilla limestones. With higher

reactivity and smaller pore diameter, Purbeck limestone is indeed expected to experience more significant effects of intraparticle mass transfer on observed rate of reaction.

An interesting result from this study was that the $f(X)$ function determined from the measurements on the Compostilla limestone has been applied successfully in modelling the conversion of the Purbeck limestone. This implies that the evolution of the pore structure of both limestone particles are similar during calcination. One hypothetical reason for this observation is related to the cycling process of the limestones, where the change of pore structure become more stable as number of cycles increases. In fact, a study of the sulphation rate of cycled lime particles showed that different limestones followed a very similar conversion *vs.* time evolution after 50 cycles [44], which indicates that the cycling process does affect how the pore structure evolves with conversion.

6 Conclusions

It has been proposed that a simple arbitrary function $f(X)$, determined from experimental measurements of rate *vs.* conversion in the kinetically-controlled regime, could be used in place of mathematical pore models to describe the evolution of pore structure during a reaction that is influenced by intra-particle gas mass transfer. A model has been constructed using the Cylindrical Pore Interpolation Model for intraparticle mass transfer, first order rate equations of calcination, the Stefan-Maxwell equations for external mass transfer and the equations of energy. The model was solved numerically by orthogonal collocation on finite elements in MATLAB. The predicted results were compared with experimental measurements conducted using two size fractions of Compostilla (after 8 cycles) and Purbeck (after 6 cycles) limestones.

The results have shown that for the calcination of limestones, the empirically-determined $f(X)$ can be successfully applied to predicting the conversion of particles of various sizes across different temperature. In addition, it was found that the $f(X)$ determined from Compostilla limestones was successful in predicting the conversion of Purbeck limestones, which indicated that the two limestones had similar evolution of pore structure during calcination. This observation was attributed to the hypothesis that the calcination – carbonation cycling process might have significantly reduced the difference in the pore structures of the limestone particles and made them more homogenous.

The significance of this research is that the $f(X)$ concept presents a simple solution in modelling the evolution of pore structures during reactions of particles. Instead of using complicated mathematical pore models, one could determine the $f(X)$ from the experiments used for kinetic studies. This idea could be further applied to many other gas-solid reactions that involve change of pore structures during reactions. One needs to be aware of

the influence of multiple types of active sites which could lead to incorrect predictions. However, multiple sites are also not reflected in most published pore models.

Acknowledgements

The authors would like to thank Felix Donat, Wenting Hu and Zlatko Saracevic from the Department of Chemical Engineering and Biotechnology University of Cambridge for their assistance with the experimental work, and Peng Dai's family for financial support. Belén González acknowledges the EU Research Fund for Coal and Steel (project number RFCR-CT-2012- 00008).

References

[1] O. Levenspiel, Chemical reaction engineering, 3rd ed., John Wiley & Sons, New York, 1999.

[2] M. Kawahata, P.L. Walker, Mode of porosity development in activated anthracite, Elsevier, 1963. doi:10.1016/B978-0-08-009708-4.50026-2.

[3] S.K. Bhatia, D.D. Perlmutter, A random pore model for fluid-solid reactions: I. Isothermal, kinetic control, AIChE J. 26 (1980) 379–386. doi:10.1002/aic.690260308.

[4] J. Szekely, J.W. Evans, A structural model for gas—solid reactions with a moving boundary, Chem. Eng. Sci. 25 (1970) 1091–1107. doi:10.1016/0009-2509(70)85053-9.

[5] M. Hartman, R.W. Coughlin, REACTION OF SULFUR DIOXIDE WITH LIMESTONE AND THE GRAIN MODEL., AIChE J. 22 (1976) 490–498.

[6] W. Liu, J.S. Dennis, D.S. Sultan, S.A.T. Redfern, S.A. Scott, An investigation of the kinetics of CO2 uptake by a synthetic calcium based sorbent, Chem. Eng. Sci. 69 (2012) 644–658. doi:10.1016/j.ces.2011.11.036.

[7] G.R. Gavals, A random capillary model with application to char gasification at chemically controlled rates, AIChE J. 26 (1980) 577–585. doi:10.1002/aic.690260408.

[8] G.A. Simons, M.L. Finson, The Structure of Coal Char: Part I—Pore Branching, Combust. Sci. Technol. 19 (1979) 217–225. doi:10.1080/00102207908946882.

[9] J. Khinast, G.F. Krammer, C. Brunner, G. Staudinger, Decomposition of limestone: The influence of CO2 and particle size on the reaction rate, Chem. Eng. Sci. 51 (1996) 623–634. doi:10.1016/0009-2509(95)00302-9.

[10] R.C. Everson, H.W.J.P. Neomagus, R. Kaitano, R. Falcon, V.M. du Cann, Properties of high ash coal-char particles derived from inertinite-rich coal: II. Gasification kinetics with carbon dioxide, Fuel. 87 (2008) 3403–3408. doi:10.1016/j.fuel.2008.05.019.

[11] S.L. Singer, A.F. Ghoniem, An Adaptive Random Pore Model for Multimodal Pore Structure Evolution with Application to Char Gasification, Energy & Fuels. 25 (2011) 1423–1437. doi:10.1021/ef101532u.

[12] P. Dai, J.S. Dennis, S.A. Scott, Using an experimentally-determined model of the evolution of pore structure for the gasification of chars by CO2, Fuel. 171 (2016) 29–43. doi:10.1016/j.fuel.2015.12.041.

[13] M.A. Saucedo, J.Y. Lim, J.S. Dennis, S.A. Scott, CO2-gasification of a lignite coal in the presence of an iron-based oxygen carrier for chemical-looping combustion, Fuel. 127 (2014) 186–201. doi:10.1016/j.fuel.2013.07.045.

[14] J.S. Dennis, A.N. Hayhurst, The effect of CO2 on the kinetics and extent of calcination of limestone and dolomite particles in fluidised beds, Chem. Eng. Sci. 42 (1987) 2361–2372. doi:10.1016/0009-2509(87)80110-0.

[15] F. García-Labiano, A. Abad, L.F. de Diego, P. Gayán, J. Adánez, Calcination of calcium-based sorbents at pressure in a broad range of CO2 concentrations, Chem. Eng. Sci. 57 (2002) 2381–2393. doi:10.1016/S0009-2509(02)00137-9.

[16] I. Barin, G. Platzki, Thermochemical data of pure substances, 3rd ed., VCH, Weinheim ; New York, 1995. doi:10.1002/9783527619825.

[17] C.Y. Wen, Y.H. Yu, A generalized method for predicting the minimum fluidization velocity, AIChE J. 12 (1966) 610–612. doi:10.1002/aic.690120343.

[18] K.B. Bischoff, Accuracy of the pseudo steady state approximation for moving boundary diffusion problems, Chem. Eng. Sci. 18 (1963) 711–713. doi:10.1016/0009-2509(63)85050-2.

[19] C.Y. Wen, NONCATALYTIC HETEROGENEOUS SOLID-FLUID REACTION MODELS, Ind. Eng. Chem. 60 (1968) 34–54. doi:10.1021/ie50705a007.

[20] R.B. Evans, G.M. Watson, E.A. Mason, Gaseous diffusion in porous media at uniform pressure, J. Chem. Phys. 35 (1961) 2076. doi:10.1063/1.1732211.

[21] L.B. Rothfeld, Gaseous counterdiffusion in catalyst pellets, AIChE J. 9 (1963) 19–24. doi:10.1002/aic.690090105.

[22] P. Schneider, Multicomponent isothermal diffusion and forced flow of gases in capillaries, Chem. Eng. Sci. 33 (1978) 1311–1319. doi:10.1016/0009-2509(78)85112-4.

[23] D. Arnošt, P. Schneider, Dynamic transport of multicomponent mixtures of gases in porous solids, Chem. Eng. J. Biochem. Eng. J. 57 (1995) 91–99. doi:10.1016/0923-0467(94)02900-8.

[24] J.B. Young, B. Todd, Modelling of multi-component gas flows in capillaries and porous solids, Int. J. Heat Mass Transf. 48 (2005) 5338–5353. doi:10.1016/j.ijheatmasstransfer.2005.07.034.

[25] J.Y. Lim, J.S. Dennis, Modeling reaction and diffusion in a spherical catalyst pellet using multicomponent flux models, Ind. Eng. Chem. Res. 51 (2012) 15901–15911. doi:10.1021/ie302528u.

[26] R. Bird, W. Stewart, E. Lightfoot, Transport phenomena, 2nd ed., John Wiley & Sons, Inc., New York, 2007.

[27] D. Green, R. Perry, Perry's chemical engineers' handbook, 8th ed., McGraw-Hill Professional, New York, 2007. doi:10.1036/0071422943.

[28] R.S. Cunningham, C.J. Geankoplis, Effects of Different Structures of Porous Solids on Diffusion of Gases in the Transition Region, Ind. Eng. Chem. Fundam. 7 (1968) 535–542. doi:10.1021/i160028a002.

[29] A. Zoia, C. Latrille, Estimating apparent diffusion coefficient and tortuosity in packed sand columns by tracer experiments, J. Porous Media. 14 (2011) 507–520. doi:10.1615/JPorMedia.v14.i6.40.

[30] A. Hayhurst, M. Parmar, Measurement of the mass transfer coefficient and sherwood number for carbon spheres burning in a bubbling fluidized bed, Combust. Flame. 130 (2002) 361–375. doi:10.1016/S0010-2180(02)00387-5.

[31] R. Jackson, Transport in porous catalysts, in: Chem. Eng. Monogr., Elsevier Scientific Pub. Co., New York, 1977.

[32] D. Alvarez, M. Peña, A.G. Borrego, Behavior of different calcium-based sorbents in a calcination/carbonation cycle for CO2 capture, Energy & Fuels. 21 (2007) 1534–1542. doi:10.1021/ef060573i.

[33] Y. Wu, J. Blamey, E.J. Anthony, P.S. Fennell, Morphological changes of limestone sorbent particles during carbonation/calcination looping cycles in a thermogravimetric analyzer (TGA) and reactivation with steam, Energy and Fuels. 24 (2010) 2768–2776. doi:10.1021/ef9012449.

[34] J.F. Davidson, D. Harrison, Fluidised Particles, Cambridge University Press, Cambridge, 1963.

[35] R.C. Darton, R.D. LaNauze, J.F. Davidson, D. Harrison, Bubble growth due to coalescence in fluidised beds, Trans Inst Chem Eng. 55 (1977) 274–280.

[36] A.N. Hayhurst, The mass transfer coefficient for oxygen reacting with a carbon particle in a fluidized or packed bed, Combust. Flame. 121 (2000) 679–688. doi:10.1016/S0010-2180(99)00178-9.

[37] P.W. Chang, B. Finlayson, Orthogonal collocation on finite elements, Math. Comput. Simul. 20 (1978) 83–92. doi:10.1016/0378-4754(78)90031-9.

[38] A.B. Fuertes, G. Marban, F. Rubiera, Kinetics of thermal decomposition of limestone particles in a fluidized bed reactor, Chem. Eng. Res. Des. 71 (1993) 421–428.

[39] R.H. Borgwardt, Calcination kinetics and surface area of dispersed limestone particles, AIChE J. 31 (1985) 103–111. doi:10.1002/aic.690310112.

[40] M.S. Murthy, B.R. Harish, K.S. Rajanandam, K.Y. Ajoy Pavan Kumar, Investigation on the kinetics of thermal decomposition of calcium carbonate, Chem. Eng. Sci. 49 (1994) 2198–2204. doi:10.1016/0009-2509(94)E0015-I.

[41] J. Zawadzki, S. Bretsznajder, Concerning the temperature increment of the rate of reaction in reactions of the type A(solid)= B-solid+C-gas, ZEITSCHRIFT FUR ELEKTROCHEMIE UND Angew. Phys. CHEMIE. 41 (1935) 215–223.

[42] W. NITSCH, UBER DIE DRUCKABHANGIGKEIT DER CACO3-BILDUNG AUS DEM OXYD, ZEITSCHRIFT FUR ELEKTROCHEMIE. 66 (1962) 703–708.

[43] S.K. Bhatia, D.D. Perlmutter, Effect of the product layer on the kinetics of the CO2-lime reaction, AIChE J. 29 (1983) 79–86. doi:10.1002/aic.690290111.

[44] B. Arias, J.M. Cordero, M. Alonso, J.C. Abanades, Sulfation rates of cycled CaO particles in the carbonator of a Ca-looping cycle for postcombustion CO2 capture, AIChE J. 58 (2012) 2262–2269. doi:10.1002/aic.12745.

Using an experimentally-determined model of the evolution of pore structure for the calcination of cycled limestones

Peng Dai*, Belén González, John S. Dennis

University of Cambridge, Department of Chemical Engineering and Biotechnology, New Museums Site, Pembroke Street, Cambridge, CB2 3RA, United Kingdom

Corresponding author

* Phone: +44(0)1223 336633. Email: pd337@cam.ac.uk

Abstract

A pseudo-steady state model of reaction and diffusion has been constructed to model the non-isothermal calcination of limestone particles which have been subjected to a history of cycling between the calcined and carbonated states. This typically occurs when using Ca-based materials for removing CO_2 from the flue gas of plants such as a power station, cement plant and steel factory in certain schemes for carbon capture and storage. The model uses a Cylindrical Pore Interpolation Model to describe the intraparticle mass transfer of CO_2 through the pores of the material coupled with an experimentally-determined function, $f(X)$, describing the pore evolution as a function of the conversion of the $CaCO_3$ present to CaO. The intrinsic rate of calcination was taken to be first order in concentration driving force. External to the limestone particle, the Stefan-Maxwell equations were used to describe the diffusion of CO_2 away from the particle and into the particulate phase of the fluidised bed. The equation of energy was used to allow for the enthalpy of the reaction. In order to validate the use of the $f(X)$ function, the theoretical predictions were compared with experiments conducted to measure the rates and extent of conversion, at various temperature and different particle sizes, of Purbeck and Compostilla limestones that had been previously cycled between the carbonated and fully-calcined state. Excellent agreement between experiment and theory was obtained, and the model using the $f(X)$ approach predicted the conversion of particles of various sizes well at temperatures different to that at which the function was derived, thus indicating that the $f(X)$ solely dependent on the evolution of the morphology of the particle.

Keywords

Calcium looping; Modelling; Calcination; Pore evolution;

List of symbols

A_A, A_K, A_C	Coefficients in pressure gradient equation	Pa s m $g^{-0.5}$ $mol^{-0.5}$
$A_{s,0}$	Initial pore area per unit mass	m^2 g^{-1}
$C_{p,n}$	Molar heat capacity of species *n*	J mol^{-1} K^{-1}
$D_{A,nm}$	Diffusivity at arbitrary Knudsen number, for species *n* and *m*	m^2 s^{-1}
$D_{B,nm}$	Molecular diffusivity, involving species *n* in *m*	m^2 s^{-1}
$D_{K,n}$	Knudsen diffusivity of species *n*	m^2 s^{-1}
D_{ref}	Molecular diffusivity $D_{B,12}$ at bulk condition	m^2 s^{-1}
$\overline{d_b}$	Mean bubble diameter	m
E_a	Activation energy	kJ mol^{-1}
H_n	Partial molar enthalpy of species *n*	J mol^{-1}
H_f	Partial molar enthalpy of formation	J mol^{-1}
h	Bed height	m
h_{mf}	Bed height at minimum fluidisation	m
J_n	Total molar flux of species *n*	mol m^{-2} s^{-1}
k_c	Rate constants of calcination reaction	mol m^{-2} s^{-1}
k_c'	Modified rate constants of calcination reaction	s^{-1}
k_0	Arrhenius coefficient of rate constant k_c'	s^{-1}
$\bar{k}$	Rate constant of carbonation reaction	m s^{-1}
M_n	Molecular mass of species *n*	g mol^{-1}
P	Total pressure	bar
P_{bulk}	Bulk pressure	bar
$p_{\mathrm{CO_2}}\|_r$	Local partial pressure of CO_2	bar
$p_{\mathrm{CO_2}}^{\mathrm{bulk}}, p_{\mathrm{CO_2}}^{eq}$	Bulk and equilibrium partial pressure of CO_2	bar
q_{c}	Intrinsic rate of calcination per unit of surface area	mol m^{-2} s^{-1}
Q_n	Net rate of change of species *n* inside the particle	mol m^{-3} s^{-1}
r	Radial distance from the particle centre	m
r_p	Radius of a limestone particle	m
r_{pore}	Mean radius of the pore	nm
R	Universal gas constant	kJ mol^{-1} K^{-1}
t	Time	s
T	Absolute temperature	K
T_{bulk}	Bulk temperature	K
U_b	Bubble velocity	m s^{-1}
U_{mf}	Flow velocity at minimum fluidisation	m s^{-1}
u_M	Mass-averaged velocity	m s^{-1}
$V_{M,\mathrm{CaO}}$	Molar volume of CaO	m^3 mol^{-1}
$V_{M,\mathrm{CaCO_3}}$	Molar volume of $CaCO_3$	m^3 mol^{-1}
X	Solid conversion	-
y_n	Mole fraction of species *n*	-
Greek letters		
Λ_{k_c}	Pre-exponential coefficient of the rate constant k_c	mol m^{-2} s^{-1}
λ_{eff}	Effective thermal conductivity of the particle	W m^{-1} K^{-1}
ε_0	Initial porosity of the particle	-
ε_b	Bubble fraction	-
ε_{bed}	Porosity of the fluidised bed around the particle	-
$\varepsilon(X)$	Porosity of the particle as a function of conversion	-
ρ_e	Bulk density of a particle	kg m^{-3}
ρ_m	Skeletal density of the particle	kg m^{-3}
τ^2	Tortuosity factor of the particle	-

τ_{bed}^2	Tortuosity factor of the fluidised bed	-
δ	External diffusion boundary layer thickness	m
η_r	Dimensionless radius	-
v_{mix}	Kinematic viscosity of gas mixture	$m^2\ s^{-1}$
v_n	Stoichiometric coefficient of species *n*	-
Subscripts		
n=1, 2	CO_2 and N_2	
Abbreviation		
BET	Brunauer–Emmett–Teller	
CPIM	cylindrical pore interpolation model	
DGM	dusty gas model	
MPTM	mean pore transport model	
OCFE	orthogonal collocation on finite element	
RPM	random pore model	

1 Introduction

Broadly-speaking, two classes of model exist to describe the non-catalytic reaction between a gas and a solid, namely the Shrinking Core Model (SCM) and the Continuous Reaction Model (CRM). The SCM has been commonly used to describe, for example, the calcination of non-porous, virgin particles of limestone (generally close to pure $CaCO_3$), where the reaction occurs at a sharp front which recedes towards the centre of the particle [1]. Generally, the rate of reaction might be limited variously by (i) chemical kinetics, (ii) diffusion through the porous product layer, (iii) transport of heat to or from a reaction interface, or (iv) diffusion through the external gas film. On the other hand, the CRM is a better description where there is slow reaction of a gas, and, or, transfer of heat, within a porous solid across a broad front or the entire particle [1]. **Fig. 1** shows the difference in local conversion profiles between two models at fixed average conversion of particle. The calcination of cycled, as opposed to virgin, limestone, possesses the characteristics of the CRM, where the initially-porous particles, containing a mixture of $CaCO_3$ and unreacted CaO, become more porous as the $CaCO_3$ is calcined to CaO during thermal decomposition. Such particles are created when raw limestone particles have been subjected to a history of cycling between the calcined and carbonated states. This typically would occur when using such Ca-based materials for removing CO_2 from the flue gas of plants such as a power station, cement plant and steel factory in certain schemes for carbon capture and storage. The present work is concerned with these cycled particles.

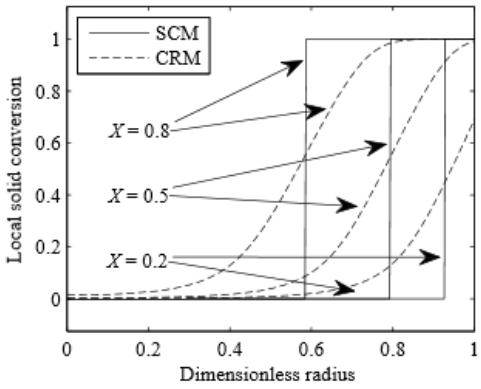

Fig. 1. Local conversion profiles of shrinking core model (SCM) and continuous reaction model (CRM) for fixed average conversion of particle.

A feature of most models of non-catalytic reactions between gases and solids generally is that the intrinsic rate of reaction, r, at a local point within a solid particle is of the form $r = g(C_i, T, P) \times f(X)$ [2,3]. Here, g describes the intrinsic reaction kinetics as a function of the temperature, T, the total pressure, P, and the concentration, C_i, of the reaction gases. The term $f(X)$ is a direct function of the conversion of the particle and is correlated with the internal morphology of the particle, *e.g.* surface area, pore size, pore size distribution *etc*. at a particular conversion. In addition, $f(X)$ is not a function of C_i, T, or P.

Many researchers have sought to model the development of internal pore structure with conversion during non-catalytic gas-solid reaction. For example, Szekely & Evans [4] assumed that solid particles consisted of an array of spherical grains with the space between them making up the voids. They made the first attempt to incorporate the structural parameters such as grain size, porosity and pore size into the reaction scheme in their grain model. Their original model assumed that the pore structure was unaffected by the progress of reaction, although later variants [5] were able to account for change in grain size with reaction. More recently, Liu *et al.* [6] developed an overlapping grain model using a fitted size distribution of grains to account for the evolution of pore structures during reaction. On the other hand, random pore models have been developed, *e.g.* Bhatia & Perlmutter [3] and Gavalas [7], using different approaches based on cylindrical pore assumptions, to model the total surface area at any conversion as a function of the initial morphological parameters, *e.g*. the initial porosity. In a somewhat different approach, Simons & Finson [8] built a mass transport model using statistical methods to specify the pore structure as a continuously branching tree. However, in his model the small pore trees will be kinetically limited while the larger pore trees are diffusion limited. This is the opposite of one might expect for pores with uniform length. The existing mathematical pore models such as the random pore model, statistical pore tree model and grain model contain parameters that are difficult to measure and thus become fitting parameters, *e.g.* the diffusivity of SO_2 through a layer of $CaSO_4$, which are complicated and equally arbitrary. In many cases, the use of mathematical pore models leads to the need to modify the original models in order to fit experimental measurements [9–11].

On the other hand, the experimentally-determined $f(X)$ function from the common measurements of reaction rate and conversion offers a straightforward method to describe the change of internal morphology at a local point within the particle being reacted under conditions affected by intraparticle mass transfer [12]. This is exemplified by recent studies of char gasification in a fluidised bed [12,13], where it was found that a simple, arbitrary function, $f(X)$, could be determined from the plot of measurements of rate *vs.* conversion of the solid char in the kinetically-controlled regime. It was proposed that the ratio between the rate of reaction at any conversion and the initial rate of reaction reflects, generally, the variation in the pore structure as the reaction proceeds in the absence of intraparticle mass transfer limitation (*e.g*. at low temperature or using small particles or with particles of low reactivity) [13], thus giving $f(X) = r(X)/r(X = 0)$.

Dai *et al.* [12] concluded that the application of the $f(X)$ concept to the gasification of chars by CO_2 suffered the complication of there being multiple types of active sites for adsorption on the surface of char so that a single $f(X)$ determined from experimental measurements at a low temperature was unable to fit satisfactorily all the measurements made at a substantially higher temperature. Accordingly, to investigate the basic hypothesis that

a gas-solid reaction can be characterised by $r = g(C_i, T, P) \times f(X)$, it is important to identify a solid which is unlikely to contain sites which vary in relative activity with temperature. The conversion of calcium carbonate to calcium oxide does not involve gas adsorption, thus limestones is a potential suitable candidate. Of course, as noted above, virgin limestone ($CaCO_3$) is almost non-porous, and the calcination reaction usually follows a shrinking core mechanism [14,15], unsuitable for the application of the $f(X)$ concept. However, limestones which have been successively calcined to CaO and carbonated in CO_2 back to $CaCO_3$ many times, present a different type of porous solid, which can be described by a CRM, as noted above. This is because the recarbonation is never complete and so after many cycles, the starting, carbonated material is, in fact, quite porous and so provides an appropriate candidate for verifying the $f(X)$ hypothesis. The purpose of this paper is therefore to examine if the $f(X)$ concept can be used for modelling non-catalytic gas – solid reactions, other than those involving gasification, using calcination as an example for different particle sizes and over a range of temperatures.

2 Experimental

2.1 Materials

Table 1. Composition of the fresh limestones in wt%.

Component	Ca	Fe	Mg	Ni	Al	K	Mn	Si	S	Zr	Sr	Ti
Compostilla	89.70	2.50	0.76	0	0.16	0.46	0	0.07	0	0	0	0.37
Purbeck	97.67	0.49	0.61	0	0.21	0.09	0.14	0.65	0.11	0.05	0	0

The gases used in the experiments were N_2 (≥ 99.9 vol%, oxygen ≤ 2 ppmv) and CO_2 (≥ 99.8 vol%). All gas cylinders were supplied by BOC or Air Liquide. Natural, uncrushed silica sand (fraction C, David Ball Group plc., dry), sieved to 355 – 425 μm, was used as a fluidised bed material. The density of the non-porous sand particles was ~ 2690 kg m^{-3}. Two types of limestone particles were used: (i) a Spanish limestone (Compostilla) after 8 cycles of calcination and carbonation, and (ii) a British limestone (Purbeck) after 6 such cycles. The number of cycles was chosen so that the particles become porous and the ultimate CO_2 uptake by the limestones of the current cycle was close to that of the previous cycle. The compositions of the fresh limestones are shown in **Table 1**. After cycling, the internal pores of the limestone, even at the start in the fully-carbonated state, were macro-pores (> 50nm) so that the calcination would likely occur continuously throughout the entire particle, as shown in **Table 2**. The cycling of the limestone particles was conducted in a bed of sand fluidised by 15 vol% CO_2 balance N_2 at 1 atm. The limestone particles were calcined at 1173 K for 10 minutes and then carbonated at 923 K for 10 minutes. Here, the temperature at which a partial pressure of CO_2 of 0.15 atm is in thermodynamic

equilibrium with a mixture of CaO and $CaCO_3$ was calculated to be 1053 K [16]. The resulting carbonated particles were cooled in a desiccator and then were sieved from the sand. Two sieve size fractions were used in the experiments for each type of limestone: 710 – 850 μm and 1400 – 1700 μm. These sizes were selected in order to recover the cycled particles effectively from the sand and to compare the theoretical predications across different particle size.

2.2 Fluidised bed experiments

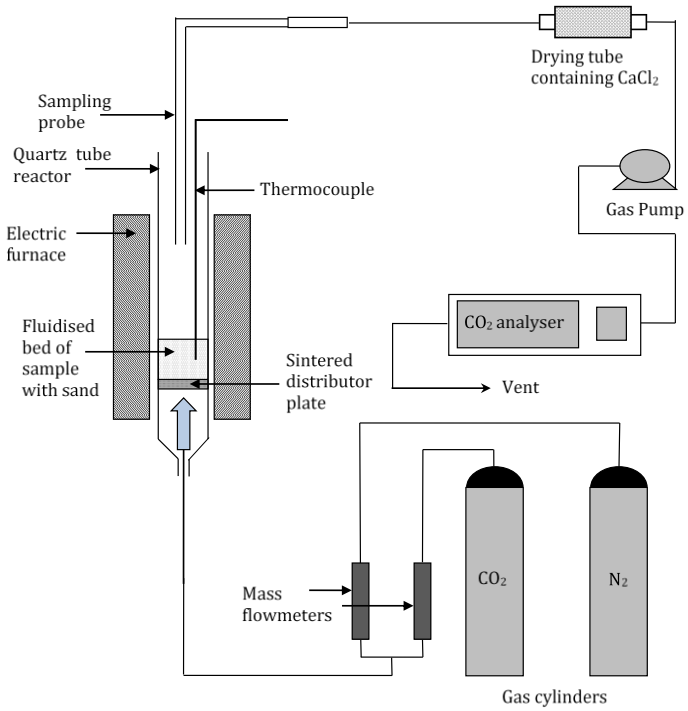

Fig. 2. Schematic diagram of the arrangement for batch experiments in a quartz reactor (i.d. 30 mm).

Batch experiments were performed in a fluidised bed contained in a quartz reactor, internal diameter 30 mm and length 460 mm, provided with a porous frit (4 mm thick, pore size 100 – 160 μm) as the distributor, situated 110 mm from the base of the reactor. By using pressure taps at the inlet and the outlet, the pressure drop across the distributor and a 20 ml sand bed was measured to be 13 – 15 mbar at experimental conditions. The reactor was externally heated by an electric furnace. The temperature of the bed was measured by a K-type thermocouple (2 mm dia.) inserted into the top, with its tip 20 mm above the distributor. Flowrates of N_2 were controlled by a mass flow meter calibrated at 293 K and 1 bar. The off-gas leaving the fluidising bed was sampled at 16.7 mL s^{-1} (STP) through a quartz tube. To prevent elutriated particles and water vapour in the sampled gas entering the analysers, the gas was passed through a glass wool filter and a drying tube filled with $CaCl_2$ in series. The mole fractions of CO_2 were measured by a non-dispersive infra-red gas analyser (ABB EL3020). Fig. 1

shows the arrangement of the apparatus. In an experiment, the reactor was filled with 20 ml of silica sand and heated to the desired temperature, *viz.* 1023 – 1173 K. For calcination, the fluidising gas was 100 mol% N_2. The total volumetric flowrate was 80 mL s^{-1} (STP), giving $U/U_{mf} \sim 6.3 – 7.9$, with U being the superficial velocity at the temperature of the bed and U_{mf} being the value at incipient fluidisation predicted from the correlation of Wen and Yu [17]. From experimental measurements using different sample masses ranging from 0.1 – 0.5 g at 1173 K, the measurement of reaction rate starts decreased when the sample mass was bigger than 0.3 g due to complications arising from mass transfer between the bubble and the particulate phases. Hence a sample mass of 0.3 g was chose for all experiments. Each experiment was repeated at least 3 times. To ensure complete calcination of the limestones, the calcination experiment is ended 10 seconds after the measured concentration of CO_2 of the off-gas returns to zero.

2.3 Characterisation of the limestone particles

Table 2. Particle characterisation of fully carbonated limestones.

Limestone	BET analysis			Mercury intrusion porosimetry					
	BET area / m^2 g^{-1}	BJH volume / cm^3 g^{-1}	BJH adsorption mean pore diameter / nm	Porosity	Total pore area / m^2 g^{-1}	Total intrusion volume / cm^3 g^{-1}	Mean pore diameter / nm	Bulk density / kg m^{-3}	Tortuosity factor / -
Compostilla, 8 cycles	0.33	7.2×10^{-3}	72	0.16	0.46	0.070	608	2235	2.8
Purbeck, 6 cycles	1.58	9.9×10^{-3}	21	0.34	3.88	0.188	190	1811	2.1

Table 2 shows the measurements from the Brunauer–Emmett–Teller (BET) analysis (TriStar 3000) and mercury intrusion porosimetry (AutoPore IV 9500), both of which produce a pore size distribution of the particles. It is clear that these cycled particles have substantial pore volume, even in their fully-carbonated state, in contrast to virgin limestone, which has negligible porosity. In the subsequent modelling, the mean pore diameter $d_{pore} = 4V/A$ from mercury porosimetry was used as the initial pore diameter of the particles, where V is the total intrusion volume and A is the total pore area. It should be noted that the limestone particles may have considerable unmeasured surface area and pore volume in the micro-porous range ($d_{pore} < 2$ nm), as the BET and mercury intrusion analyser were unable to measure pore diameters smaller than 1.7 nm and 3 nm respectively.

Dai *et al.* [12] measured the particle size distribution of 600 – 1000 μm dia. char particles with the same sub-angular shape to the limestone particles by optical microscopy and showed that the effective particle diameter

$D(3,2) \times \psi$, where $D(3,2)$ was the Sauter mean diameter and ψ is a shape factor, is very close to the geometric mean of the mesh sizes. Therefore in the model, the mean, external particle diameter d_p was calculated from the geometric mean of the sieves d_p = (lower mesh × upper mesh)$^{0.5}$.

3 Theoretical

The model described in this work assumed that the limestone particle is spherical and is calcined in a bed of silica sand fluidised by a stream of N_2. The only reaction occurring is:

$$CaCO_{3(s)} \rightleftharpoons CaO_{(s)} + CO_{2(g)} \qquad \Delta H^0_{298K} = +178 \text{ kJ mol}^{-1} \qquad \text{(I)}$$

The two principal assumptions were:

i) The material and energy balances inside and outside the particle are in pseudo-steady state, so that the gas concentrations, total fluxes, total pressure and temperature have no time dependence. By using the pseudo-steady state assumption here, it means that the time needed to establish an initial steady concentration profile is very small. Without this assumption, the initial concentration would have been zero everywhere. Nevertheless, as justified by Bischoff [18], the profiles generated using this assumption will be achieved very quickly in a gas-solid system. In fact, the thermal diffusivity of the solid at 800 °C is about 9×10^{-6} m^2/s, even for a 2 mm dia. particle, the time constant estimated from Radius^2 / (2 × thermal diffusivity) is very small ~ 0.2 s. Wen [19] also concluded that the pseudo-steady state solution was a good approximation for most of the solid-gas reaction systems except for systems with extremely high pressure and very low solid reactant concentration. However, the balances are affected indirectly by the conversion X which does have time dependence and affects the physical properties of the particle (*e.g.* porosity, pore diameter and particle size).

ii) The evolution of the internal morphology of a limestone particle during calcination can be described by an arbitrary $f(X)$, a function of X – the local conversion of the maximum available $CaCO_3$ content within the particle after cycling. The reason for such a definition of conversion is that the limestone particle is only partially carbonated and the maximum CO_2 uptake decays gradually with the number of cycles. Hence the reaction rate at some point within the solid can be expressed in the form of $r = g(C_i, T, P) \times f(X)$. It was assumed that $f(X)$ applies everywhere within a particle and is independent of temperature. The value of $f(X)$ changes with the local conversion, which will vary with distance from the centre of the particle. The $f(X)$ can be obtained from a plot of the experimental rate of calcination against conversion obtained from experimental measurements in which the rate is controlled *solely* by intrinsic chemical kinetics [12,13].

3.1 The kinetics of the calcination reaction

The intrinsic rate of reaction per unit of surface area for reaction (I) was given by [14]

$$-q_{\mathrm{c}} = k_c - \bar{k} C_{\mathrm{CO_2}} = k_c - \bar{k}\, p_{\mathrm{CO_2}}/RT \tag{1}$$

where k_c is the rate constant of the calcination reaction (here, in mol m^{-2} s^{-1}), $\bar{k}$ is the rate constant of the reverse, carbonation reaction (m s^{-1}) and $p_{\mathrm{CO_2}}$ is the partial pressure of CO_2. At equilibrium, the rate $q_{\mathrm{c}} = 0$, so that $k_c - \bar{k}\, p_{\mathrm{CO_2}}^{eq}/RT = 0$. Therefore, the ratio of rate constants is:

$$k_c/\bar{k} = p_{\mathrm{CO_2}}^{eq}/RT \tag{2}$$

Substituting Eq. (2) into Eq. (1),

$$-q_{\mathrm{c}} = k_c\left(1 - p_{\mathrm{CO_2}}/p_{\mathrm{CO_2}}^{eq}\right) \tag{3}$$

Here $p_{\mathrm{CO_2}}^{eq}$ is the equilibrium partial pressure of CO_2 at local conditions. Barin and Platzki [16] gave the following expression for $p_{\mathrm{CO_2}}^{eq}$:

$$p_{\mathrm{CO_2}}^{eq} = 4.083 \times 10^7 \exp(-20474/T) \tag{4}$$

where the unit of T is in K. The rate constant k_c was assumed to be an activated quantity, thus $k_c = \Lambda_{k_c} \exp\left(-E_a/RT\right)$.

Based on the assumption ii), the rate of reaction per unit volume of particle, Q_C, is:

$$Q_C = q_{\mathrm{c}} A_{s,0} \rho_{e,0} f(X) = -k_c\left(1 - p_{\mathrm{CO_2}}/p_{\mathrm{CO_2}}^{eq}\right) A_{s,0} \rho_{e,0} f(X) \tag{5}$$

where the parameter $A_{s,0}$ is the initial pore area per unit mass and $\rho_{e,0}$ is the initial bulk density of the particles.

3.2 Equations of mass balance

A pseudo-steady mass balance over a spherical shell at radius r gives the flux equations for CO_2 and N_2:

$$\frac{1}{r^2}\frac{d}{dr}\left(r^2 J_{\mathrm{n}}\right) = Q_{\mathrm{n}} = -\nu_n Q_C = -\nu_n q_{\mathrm{c}} A_{s,0} \rho_e f(X) \qquad n = 1, 2 \tag{6}$$

where J_n is the total flux (*i.e.* diffusive flux + advective flux) of species n. The parameter Q_n is the net rate of reaction of species n, in mol m^{-3} s^{-1}, which is positive for a net gain and negative for a net loss in species, and ν_n is the stoichiometric coefficient of species n in reaction (I). The subscripts 1 and 2 are used to represent CO_2 and N_2. A material balance on carbon across a differential element gives the variation of local conversion of $CaCO_3$ with respect to time:

$$\left.\frac{dX}{dt}\right|_r = -M_{\mathrm{CaCO_3}}\left(\frac{Q_C}{\rho_{e,0}}\right) = k_c A_{s,0} M_{\mathrm{CaCO_3}}\left(1 - p_{\mathrm{CO_2}}/p_{\mathrm{CO_2}}^{eq}\right) f(X) \tag{7}$$

the initial condition of which is:

$$t = 0: \quad X(r) = 0 \quad \text{for all } r \in [0, r_p] \tag{8}$$

where the particle centre is $r = 0$ and the particle surface is $r = r_p$. Since $A_{s,0}M_{\mathrm{CaCO_3}}$ is the initial pore area per unit volume of particle – a constant, the product of parameters $k_c A_{s,0} M_{\mathrm{CaCO_3}}$ can be replaced by a modified rate constant k_c':

$$\left.\frac{dX}{dt}\right|_r = k_c'\left(1 - p_{\mathrm{CO_2}}/p_{\mathrm{CO_2}}^{eq}\right) f(X)$$
$$k_c' = \Lambda_{k_c} A_{s,0} M_{\mathrm{CaCO_3}} \exp(-E_a/RT) = k_0 \exp(-E_a/RT) \tag{9}$$

The activation energy of k_c' is the same as that of k_c, but the pre-exponential becomes $k_0 = \Lambda_{k_c} A_{s,0} M_{\mathrm{CaCO_3}}$.

3.3 Equations of intraparticle mass transfer

A model of multi-component diffusion based on the Stefan-Maxwell equations within a porous medium was needed to describe the intraparticle diffusion rigorously. The two principal flux models for non-equimolar, multi-component mass transfer are the Dusty Gas Model (DGM) [20], and the Mean Pore Transport Model (MPTM) [21–23]. Given that both models are algebraically complicated, Young and Todd [24] developed a new MPTM called the Cylindrical Pore Interpolation Model (CPIM). Comparing all three models, the CPIM has a more rigorous treatment of continuum flow, a clearer interpolation procedure for transitional flow and a more compact form of the working equations which helps to clarify the roles of the governing parameters. Recent studies suggest that the CPIM is well suited to modelling multi-component diffusion in both catalyst pellets [25] and in gasifying char particles [12,13]. For this reason, the CPIM was selected to model intraparticle diffusion in the present work. The governing equations are:

$$\frac{dy_n}{dr} = \frac{\tau^2 RT}{\varepsilon P} \sum_{m=1}^{2} \left(\frac{y_n J_m}{D_{A,mn}} - \frac{y_m J_n}{D_{A,nm}} \right) \qquad n = 1, 2 \tag{10}$$

$$\frac{dP}{dr} = -\frac{\tau^2 A_A}{\varepsilon} \sum_{n=1}^{2} \left(\sqrt{M_n} \cdot J_n \right) \tag{11}$$

The boundary conditions for the above equations are given at the centre ($r = 0$) and the surface ($r = r_p$) of the particle:

$$r = 0: \quad J_1 = 0 \quad J_2 = 0 \tag{12}$$

$$r = r_p: \quad y_n = y_n^{\mathrm{surface}} \quad (n = 1, 2) \quad \& \quad P = P_{\mathrm{surface}} \tag{13}$$

Here, y_n is the mole fraction of species n, τ^2 represents the tortuosity factor of the particle from mercury intrusion porosimetry measurements, ε is the porosity at the local point, which varies with conversion and is discussed later,

and M_n is the molar mass of gas species n. The parameters $D_{A,nm}$ and A_A were found by interpolating between the extremes of continuum and Knudsen flow using the equations proposed by Young and Todd [24]:

$$\frac{1}{D_{A,nm}} = \frac{1}{D_{K,n}} + \frac{1}{D_{B,nm}} \qquad \frac{1}{A_A} = \frac{1}{A_K} + \frac{1}{A_C} \tag{14}$$

where $D_{B,nm}$ is the molecular diffusivity calculated from the Chapman-Engskog theory using the Lennard-Jones (6-12) potential [26]. The error in the predicted binary diffusivities by this method is ~ 7.3% [27]. $D_{K,n}$ is the Knudsen diffusivity and the parameters A_K and A_C are the coefficients in the pressure gradient equation in the continuum and Knudsen regime, given by [24,28]

$$D_{K,n} = \frac{2r_{pore}}{3}\sqrt{\frac{8RT}{\pi M_n}} \qquad A_K = \frac{3}{4r_{pore}}\sqrt{\frac{\pi RT}{2}}$$
$$A_C = 8\mu_{mix}RT \Big/ \left(Pr_{pore}^2 \sum_{n=1}^{2} \left(y_n \sqrt{M_n} \right) \right) \tag{15}$$

where the viscosity of the gas mixture, μ_{mix}, was calculated using Chapman-Engskog theory.

The porosity, ε, changes with the local conversion of $CaCO_3$, X, during reaction and can be derived from the volume balance equation for a thin cylindrical shell inside the particle:

$$\varepsilon(X) = \varepsilon_0 + X(1-\varepsilon_0)\left(1 - V_{m,\mathrm{CaO}}/V_{m,\mathrm{CaCO_3}}\right) \tag{16}$$

where $V_{m,\mathrm{CaO}}$ and $V_{m,\mathrm{CaCO_3}}$ are the molar volume of the non-porous CaO and $CaCO_3$ solids. In terms of the pore diameter, it was assumed that the particle has uniform cylindrical pores of initial diameter $d_{pore,0}$; the corresponding initial porosity of the particle was ε_0. Ignoring the small volume of crossing between pore channels, the local porosity can be estimated from $\varepsilon(r) \cdot \delta V = \pi d_{pore}^2 \sum_{i=1} L_i/4$, where δV is the volume of a differential element between r and $r+dr$ and $\sum_{i=1} L_i$ is the sum of the length of the cylindrical pores within the element. Assuming that the evolution of the pores during reaction occurs only in a radial direction so that the pore diameter changes while the length of the pore remains constant, then:

$$\varepsilon(r)/\varepsilon_0 = \left(d_{pore}/d_{pore,0}\right)^2 \tag{17}$$

Substituting Eq. (16) into (17), the pore diameter at some time when the local conversion is X is:

$$r_{pore} = r_{pore,0}\sqrt{\left(\varepsilon_0 + X(1-\varepsilon_0)\left(1 - V_{m,\mathrm{CaO}}/V_{m,\mathrm{CaCO_3}}\right)\right)/\varepsilon_0} \tag{18}$$

3.4 Equations of external mass transfer

The particulate phase of the fluidised bed was considered to have a constant local tortuosity and porosity around the limestone particle. It was also assumed that there is no variation of pressure with radial distance

outside the limestone particle, since the interstitial velocity of fluidising gas – ~1.1 m/s (STP) is much larger than the mass average velocity of gas leaving the surface of a reaction particle – ~0.04 m/s (STP) calculated from the gas flux at the surface. This suggests that there is no tendency to form voids or bubbles around the reacting particle in the case under consideration and that pressure variations outside the particle can be neglected. The general Stefan-Maxwell equations [26] were used to model the external mass transfer within a diffusion boundary layer of thickness δ outside the particle:

$$\frac{dy_n}{dr} = \frac{\tau_{bed}^2 RT}{\varepsilon_{bed} P} \sum_{m=1}^{2} \left(\frac{y_n J_m - y_m J_n}{D_{B,nm}} \right) \qquad n = 1,2 \qquad dP/dr = 0 \tag{19}$$

Here τ_{bed}^2 is the tortuosity factor of the sand bed. It was experimentally measured to be $1.34^2 = 1.80$ for a packed bed with 200 µm dia. quartz sand by Zoia and Latrille [29]. Also, ε_{bed} is the porosity of the bed, assumed to be 0.44, the same as the porosity at incipient fluidisation used by Hayhurst and Parmar [30] for a bubbling fluidised bed of silica sand. The parameter $D_{B,ab}$ refers to the binary molecular diffusivity of species *n* and species *m*. The boundary conditions at the particle surface ($r = r_p$) and the edge of boundary layer ($r = r_p + \delta$) are:

$$r = r_p: \quad J_1 = J_1^{\text{bulk}} \tag{20}$$

$$r = r_p + \delta: \quad y_n = y_n^{\text{bulk}} \quad (n = 1,2) \quad \& \quad P = P_{\text{bulk}} \tag{21}$$

3.5 Equations of energy balance

Outside the limestone particle, convective heat transfer in a bubbling fluidised bed involves packets of sand particles coming into contact with the limestone for a short time, then quickly moving away to be replaced by other packets. It was assumed that the heat transfer coefficient between the particulate phase of the fluidised bed and the surface of the particle was large, so that the particle surface is close to the temperature of the bulk. It was also assumed that the radiative contribution and transpiration contributions to heat transfer were small.

Inside the limestone particle, the energy flux, *E*, is given by [26]

$$E = \sum_{n=1}^{2} M_n J_n \left(\frac{u_M^2}{2} + \frac{H_n}{M_n} \right) - \lambda_{eff} \frac{dT}{dr} \tag{22}$$

Jackson [31] showed that the energy balance can be expressed as $\text{div}(E) = 0$:

$$\frac{1}{r^2}\frac{d}{dr}\left(r^2\frac{dT}{dr}\right)=\frac{1}{\lambda_{eff}}\sum_{n=1}^{2}\left(H_n+\frac{u_M^2}{2}M_n\right)Q_n+\frac{1}{\lambda_{eff}}\frac{dT}{dr}\sum_{n=1}^{2}J_nC_{p,n}$$
$$+\frac{1}{\lambda_{eff}}\sum_{n=1}^{2}M_nJ_nu_M\frac{du_M}{dr} \quad (23)$$

where $C_{p,n}$ is the molar heat capacity of species *n* and λ_{eff} is the effective thermal conductivity. H_n is the partial molar enthalpy of species *n* at temperature *T*, and is calculated from standard enthalpy of formation $H_{f,n}^0$ by $H_n = H_{f,n}^0 + \int_{298}^{T} C_{p,n}dT$. This equation makes specific allowance for the small change in momentum occurring as a result of the change in mass in the gas phase during the non-catalytic decomposition of the solid. The calculation of the thermal parameters C_p and λ is discussed in the next section. Finally, u_M is the mass-averaged velocity of the mixture which is given by $u_M = \sum_{n=1}^{2} M_nJ_n / \sum_{n=1}^{2}\rho_n$. The boundary conditions for the internal energy balance were:

$$r = 0: \quad dT/dr = 0 \qquad r = r_p: \quad T = T_{\text{bulk}} \quad (24)$$

3.6 Calculation of parameters

The initial pore area per unit mass $A_{s,0}$ was obtained from the BET area measurement of the limestone particles. The initial bulk density $\rho_{e,0}$, the initial pore diameter $d_{pore,0}$, the tortuosity factor τ^2 and the initial porosity of the particle ε_0 were determined from the mercury porosimetry measurements, as shown in **Table 2**. Alvarez *et al.* [32] did reported up to 50% increase in pore diameter of natural limestone particles after 100 cycles. In terms of the particle size, Wu *et al.* [33] reported only 2 – 7 % reduction of particle diameter after 10 calcination – carbonation cycles. Hence in this study the overall particle size was assumed to be constant during calcination. Any change of the solid volume due to the difference in molar volumes of $CaCO_3$ and CaO was taken only to affect the pore structure parameters *e.g.* porosity and pore diameter.

The boundary layer thickness δ was given by Hayhurst and Parmar [30]:

$$\text{Sh}_{\text{EMCD}} = 2\varepsilon_{mf}(1 + r_p/\delta) \quad (25)$$

$$\text{Sh}_{\text{EMCD}} = 2\varepsilon_{mf} + 0.61\left(2r_pU_p/\upsilon_{mix}\right)^{0.48}\left(\upsilon_{mix}/D_{B,12}\right)^{0.33} \quad (26)$$

$$U_p = U_{mf}(1-\varepsilon_b)\{1 - 0.5\pi\text{Ln}(1 - 6\varepsilon_b/\pi)\} \quad (27)$$

where $\varepsilon_{mf} = 0.44$ was the voidage at incipient fluidisation for a bubbling fluidised bed with silica sand used by Hayhurst and Parmar [30]. Also, υ_{mix} is the kinematic viscosity of the gas mixture calculated using Chapman-Engskog theory and $D_{B,12}$ the binary molecular diffusivity for CO_2 and N_2. The bubble fraction ε_b was given by

$\varepsilon_b = (U - U_{mf})/U_b = (h - h_{mf})/h$, where $U_b = (U - U_{mf}) + 0.71(g\overline{d_b})^{0.5}$ [34]. Here, h_{mf} was the bed height at incipient fluidisation, measured to be 0.029 m and $\overline{d_b}$ was the mean bubble diameter estimated from the correlation of Darton *et al.* [35]: $\overline{d_b} = 0.54(U - U_{mf})^{0.4} h^{0.8}/(2g^{0.2})$ with h being the expanded height of the bed when fluidised at superficial velocity U. Although the correlation was based on equimolar counter-diffusion (EMCD), it has been shown that it will yield the correct value of δ from Eq. (25), even for non-EMCD [36].

The thermal conductivities of the gases were calculated from $\lambda = C_1 T^{C_2}/(1 + C_3/T + C_4/T^2)$, where $C_1 - C_4$ are constants [27]. The effective thermal conductivity of the particle was calculated from $\lambda_{eff} = (1 - \varepsilon)\lambda_{solid} + \varepsilon\lambda_{gases}$, where $\lambda_{gases} = \sum_1^{a=3} y_a \lambda_a$. The overall thermal conductivity was largely influenced by that of the solid. The reported thermal conductivity of limestone ($CaCO_3$) and lime (CaO) is 2.25 and 0.84 W m^{-1} K^{-1} respectively [27]. The exact mole fraction of $CaCO_3$ and CaO within the particles after cycling was unknown, hence, λ_{solid} was taken to be 1.5 W m^{-1} K^{-1}. The specific heat capacity of each gas was estimated from $C_p = E_1 + E_2 T + E_3/T^2$, where $E_1 - E_3$ are constants from Green and Perry [27].

3.7 Numerical solution

The system is described by Eq. (6) to (24). Both the intraparticle and external mass transfer models have five 1st order ordinary differential equations (ODEs) in the space domain, and hence five boundary conditions are provided. The ODE for conversion is 1st order in the time domain, hence only one initial condition is required. The energy equation is a 2nd order ODE, hence two boundary conditions are required for both the internal and external cases.

The main difficulty in solving the system lies in efficient solution of the large system of equations. A numerical algorithm, Orthogonal Collocation on Finite Elements (OCFE) [37] was written in MATLAB to solve the model. Pseudo-steady state was assumed for all the other variables except for the conversion X. Using the initial condition in Eq. (8), the 1st order time-dependent ODE of local conversion X, Eq. (7), was solved. The value of $X(\eta_r)$ at time $t + \Delta t$ could be calculated based on $X(\eta_r)$ and dX/dt at time t. The relevant model parameters (*e.g.* porosity and pore diameter) were updated with the new value of $X(\eta_r)$, and then the internal and external models were solved for results at time $t + \Delta t$. The iterative process was stopped when the overall conversion reached unity.

Since the model predicts the distributions of reaction rate and conversion across the radius of a particle, the overall values of rate and conversion need to be obtained from integration across the particle radius. For a

distribution of χ (*e.g.* Q_C and X), its volume averaged value can be calculated from $\bar{\chi} = 3\int_0^1 ({\eta_r}^2\chi)d\eta_r$, where η_r is the dimensionless radius used inside the particle. The integral was evaluated numerically.

4 Results

Fig. 3 shows the raw measurements of CO_2 mole fraction in the off-gas during the calcination of cycled Compostilla (plot a) and Purbeck limestone particles (plot b) in a bed of silica sand fluidised by pure N_2. The figure suggests that the calcination of Compostilla at 1173 K was completed after ~ 50 s while Purbeck at 1173 K finished calcining after 35 s. The peak concentration of CO_2 from Compostilla was about half that of Purbeck, hence the reactivity of Compostilla was significantly less than that of Purbeck. The equilibrium partial pressure of CO_2 at 1173 K is about 1.087 bar, so the concentration driving force $p_{CO_2}/p_{CO_2}^{eq} < 5\%$. Hence this confirms that the fluidised bed was close to a differential reactor, and it is reasonable to use 0% CO_2 as the bulk concentration in the model.

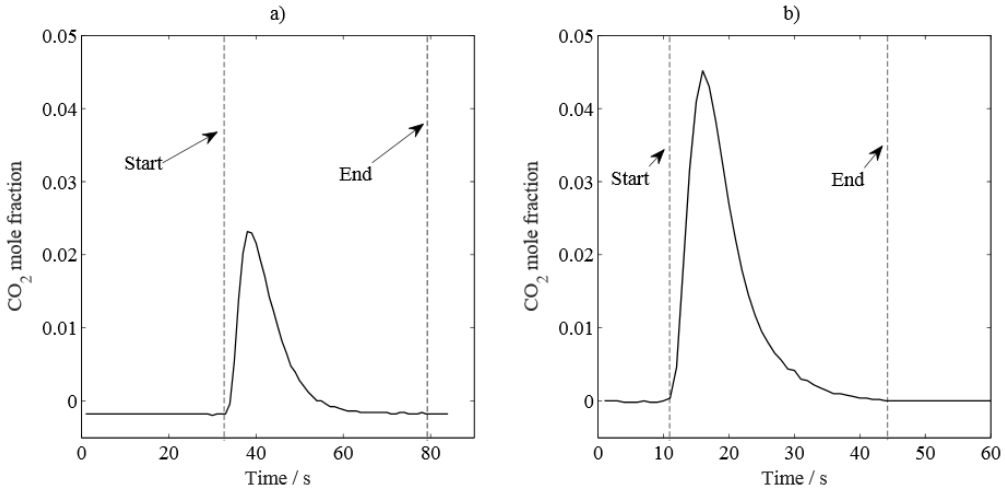

Fig. 3. Measurements of CO_2 mole fraction during calcination of cycled limestones at atmospheric pressure: a) Compostilla 8 cycles 0.71 – 0.85 mm at 1173 K; b) Purbeck 6 cycles 0.71 – 0.85 mm at 1173 K.

The overall rate of production of CO_2 from calcination in s^{-1} is $dX/dt = \left(\dot{N}_{out}y_{CO_2,out} - \dot{N}_{in}y_{CO_2,in}\right)/\int\left(\dot{N}_{out}y_{CO_2,out} - \dot{N}_{in}y_{CO_2,in}\right)dt$. The parameters $\dot{N}_{out}$ and $\dot{N}_{in}$ are the total molar flows leaving and entering the reactor at the exit and entrance conditions, where $\dot{N}_{out}\left(1 - y_{CO_2,out}\right) = \dot{N}_{in}\left(1 - y_{CO_2,in}\right)$ from the mass balance of nitrogen. The raw measurements were deconvoluted to account for the mixing and delay in the sampling line using the method described by Saucedo *et al.* [13].

Table 3. Kinetic parameters of the calcination of 0.71 – 0.85 mm dia. limestone particles.

Limestone particles	k_0 / s^{-1}	E_a / kJ mol^{-1}

Compostilla, 8 cycles	1.72×10^{7}	175 ± 12
Purbeck, 6 cycles	6.50×10^{7}	186 ± 5

The Arrhenius coefficients and activation energies of the kinetic parameter k_c' in Eq. (9), shown in Table 3, were determined from the initial rate extrapolated from the experimental measurements, as shown in **Fig. 4**. At the start of reaction, the particle conversion is 0 and $f(X) = 1$, and Eq. (9) can be rearranged

$$\mathrm{Ln}(dX/dt\,|_{t=0}) = -E_a/RT + \mathrm{Ln}(k_0) + \mathrm{Ln}\left(1 - p_{\mathrm{CO_2}}/p_{\mathrm{CO_2}}^{eq}\right) \quad (28)$$

If the value of $p_{\mathrm{CO_2}}/p_{\mathrm{CO_2}}^{eq}$ is much smaller than 1, which is usually the case if the reaction is controlled by intrinsic kinetics, then

$$\mathrm{Ln}(dX/dt\,|_{t=0}) = \mathrm{Ln}(k_c') = -E_a/RT + \mathrm{Ln}(k_0) \quad (29)$$

A plot of $\mathrm{Ln}(dX/dt\,|_{t=0})$ *vs.* $1/T$ should therefore yield the activation energy E_a and the Arrhenius coefficient k_0. The linearity of **Fig. 5** and **Fig. 8** in section 4.1 and 4.2 respectively show that the calcination of the limestone was indeed controlled by chemical kinetics at low temperature, hence confirming the use of Eq. (29) for the determination of the kinetic parameters. The errors associated with the kinetic parameters mainly come from extrapolating the initial rates from measurements, and using a limited number of measurements for linear regression analysis. The 95% confidence intervals of the kinetic parameters are shown in **Fig. 5** and **Fig. 8**.

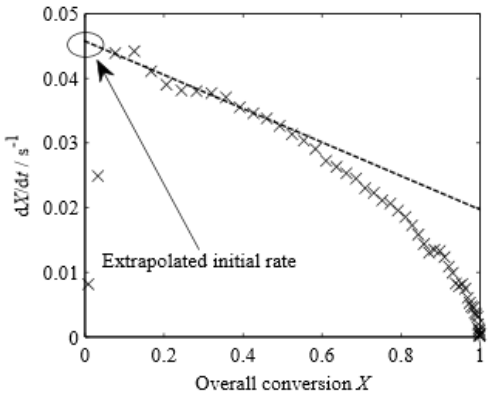

Fig. 4. Determining initial rate of reaction using linear extrapolation (--) on rate and conversion measurements (×) of Compostilla 0.71 – 0.85 mm particles (8 cycles) at 1073 K.

4.1 Calcination of Compostilla limestone particles

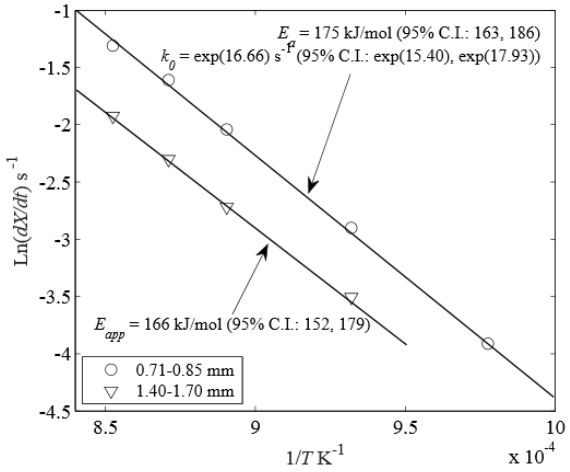

Fig. 5. Determining the kinetic parameters of Compostilla limestone particles (8 cycles). The measurements were obtained from the calcination of the limestone particles at 1023 K (0.71 – 0.85 mm only), 1073 K, 1123 K, 1148 K and 1173 K. The values of the kinetic parameters of the rate constant are shown with 95% confidence interval (C.I.).

Particles of Compostilla limestone with diameters of 0.71 – 0.85 mm and 1.40 – 1.70 mm were calcined at 1023 K (0.71 – 0.85 mm only), 1073 K, 1123 K, 1148 K and 1173 K. Using the initial rate extrapolated to zero conversion, **Fig. 5** shows that the plot of $\mathrm{Ln}(dX/dt)$ *vs.* $1/T$ of each particle forms straight lines. The values of the kinetic parameters in Eq. (9) were determined from a linear regression analysis, yielding an activation energy of $E_a = 175 \pm 12$ kJ/mol and $k_0 = 1.72 \times 10^7$ s^{-1} for 0.71 – 0.85 mm dia. particle. For 1.40 – 1.70 mm dia. particle, the reaction rates were lower than those of 0.71 – 0.85 mm dia. particle and the apparent activation energy was 166 ± 14 kJ/mol, representing a 9 kJ/mol reduction that is within an error band of ± 12 kJ/mol. It is expected that the gradient of a best fit line would approach a half of its intrinsic value if the reaction rate were significantly limited by intraparticle mass transfer [1]. However, this is not observed in **Fig. 5**. The values of the activation energy indicate that the reactions could not have been in mass transfer limited regime. Hence, it can be concluded that (i) the calcination of 0.71 – 0.85 mm dia. particles was controlled by intrinsic chemical kinetics; (ii) the reactions of 1.40 – 1.70 mm dia. particles were possibly affected by intraparticle mass transfer but not severely so.

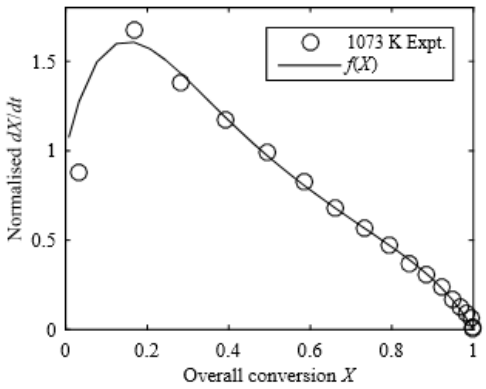

Fig. 6. Determining the function $f(X)$ from the plot of normalised rate *vs.* conversion measurement of 0.71 – 0.85 mm dia. Compostilla (8 cycles) at 1073 K.

The form of $f(X)$ needs to be determined from experimental measurements of calcination rate *vs.* conversion conducted under conditions where the reaction is controlled by intrinsic chemical kinetics. Owing to the low rate of reaction at 1023 K, the percentage fluctuation caused by random noise in the measurements of CO_2 concentration was very large. The resulting $f(X)$ was not a smooth function, as expected. However, since experiments at both 1023 K and 1073 K appear to be in the regime of chemical kinetic control, as shown in **Fig. 5**, the $f(X)$ function was determined from the measurements at 1073 K instead. **Fig. 6** shows the plot of $f(X)$, a 6^{th} order polynomial of X, determined from the normalised rate *vs.* conversion measurements of Compostilla limestone of sieve diameter 0.71 – 0.85 mm, calcined at 1073 K. The figure shows a peak higher than 1 at about 20% conversion. This is due to the fact that part of the surface area that is previously unreachable become accessible when the solid volume reduces during the initial stage of calcination. This increase in surface area only occurs at low conversion when the coalescence of pores is insignificant. Using this $f(X)$, the model was able to fit well the experimental results at 1023 K, as seen in Fig. 7(a). This strongly suggests that the $f(X)$ was not merely a fit valid for one particular experimental condition.

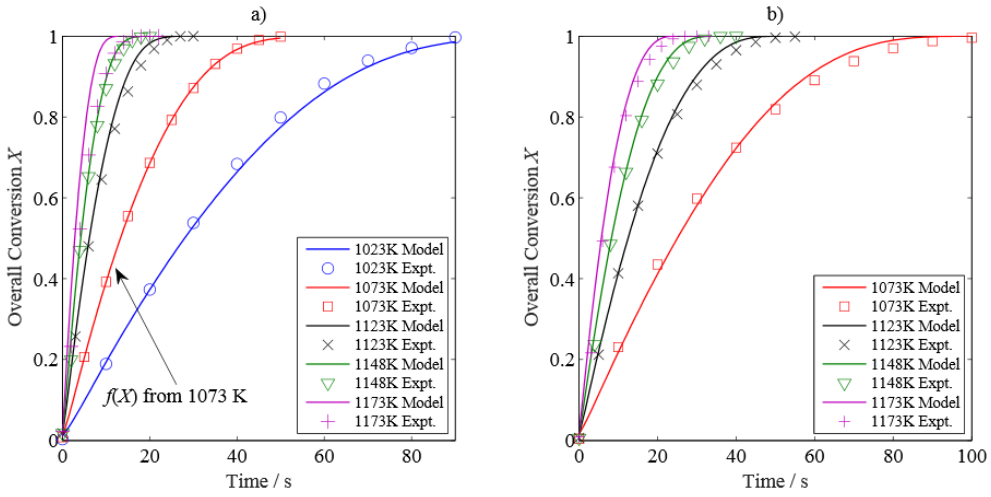

Fig. 7. Comparison of model results (lines) with experimental measurements (points) of the calcination of Compostilla limestone particles (8 cycles) by 100% N_2: a) 0.71 – 0.85 mm; b) 1.40 – 1.70 mm. The $f(X)$ was determined from the rate *vs.* conversion measurements of 0.71 – 0.85 mm particles at 1073 K, and was applied to all cases.

Further comparisons between model predictions and experimental measurements for Compostilla limestone of 0.71 – 0.85 mm dia. and 1.40 – 1.70 mm dia. are shown in **Fig. 7**, with generally good agreement being seen between experiment and theory. However, the experimental measurements for the 0.71 – 0.85 mm dia. particle at 1173 K were almost identical to those at 1148 K, which indicates either a severe limitation by external mass transfer or experimental error arising from the rapidity of the reaction and the problem in correcting for mixing in the sampling line. **Fig. 5** shows that even for the larger particles at higher temperature, the rate of reaction was not limited by mass transfer as the gradients of the two measurements are almost the same. Therefore it can be concluded that the unexpected behaviour of the rate of 0.71 – 0.85 mm dia. at 1173 K is due to error.

4.2 Calcination of Purbeck limestone particles

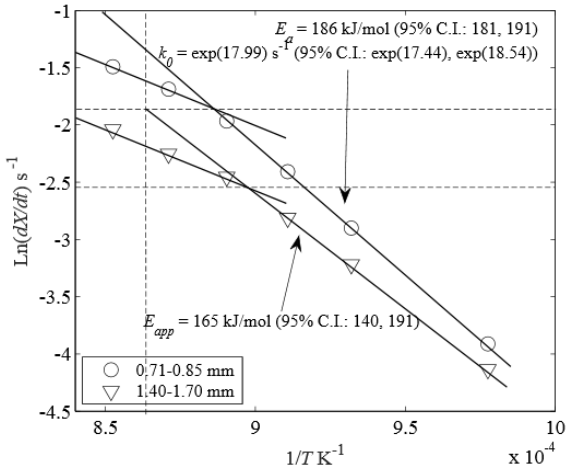

Fig. 8. Determining the kinetic parameters of Purbeck limestone particles (6 cycles). The measurements are from calcination of 0.71 – 0.85 mm and 1.40 – 1.70 mm particles at 1023 K, 1073 K, 1098 K, 1123 K, 1148 K and

1173 K. The gradient of the linear regression line for both particles reduced by ~ 50% at 1098 – 1173 K. The values of the kinetic parameters are shown with 95% confidence interval (C.I.).

Experiments with Purbeck limestone were performed using 0.71 – 0.85 mm and 1.40 – 1.70 mm dia. particles at 1023 K, 1073 K, 1098 K, 1123 K, 1148 K and 1173 K. The same kinetic analysis was performed on the experimental measurements and the results are shown in **Fig. 8**. A linear regression line of the plot of $\mathrm{Ln}(dX/dt)$ *vs.* $1/T$ gives an activation energy $E_a = 186 \pm 5$ kJ/mol and the rate constant $k_0 = 6.50 \times 10^7$ s^{-1}. At 1098 – 1173 K, the gradient of the regression lines of measurements, thus $-E_a/R$, is reduced by about half at $T >$ 1098 K. Hence, this figure suggests that the transition of the reaction regime from chemical kinetic control to mass transfer control starts at ~ 1098 K. **Fig. 8** also shows that the rates of reaction of the 1.40 – 1.70 mm dia. particles are lower than those of the 0.71 – 0.85 mm dia. particles; the linear regression lines of the 1023 – 1098 K measurements show a 21 kJ/mol decline, larger than the ± 5 kJ/mol error, in the apparent activation energy, probably owing to a growing influence of the mass transfer limitation for larger particles. At $T >$ 1098 K, the slope of the points of 1.40 – 1.70 mm dia. particle is almost the same as that of 0.71 – 0.85 mm particle, suggesting that the reaction becomes limited by mass transfer. Furthermore, for the 1.40 – 1.70 mm dia. particles the transition of the reaction regime occurs at a temperature lower than that of the 0.71 – 0.85 mm dia. particle, a consequence of the increased mass transfer limitation in larger particles.

Fig. 9 compares the rates of conversion *vs.* time from experimental measurements (points) with the theory (line) for Purbeck limestone calcined in 100% N_2 at 1023 – 1173 K. Interestingly, the $f(X)$ determined previously from the measurements on Compostilla limestone of 0.71 – 0.85 mm dia. at 1073 K, shown in **Fig. 6**, was successfully applied here for both size fractions of Purbeck limestone. The result shows that the model fits perfectly with the experimental measurements even for measurements at 1173 K.

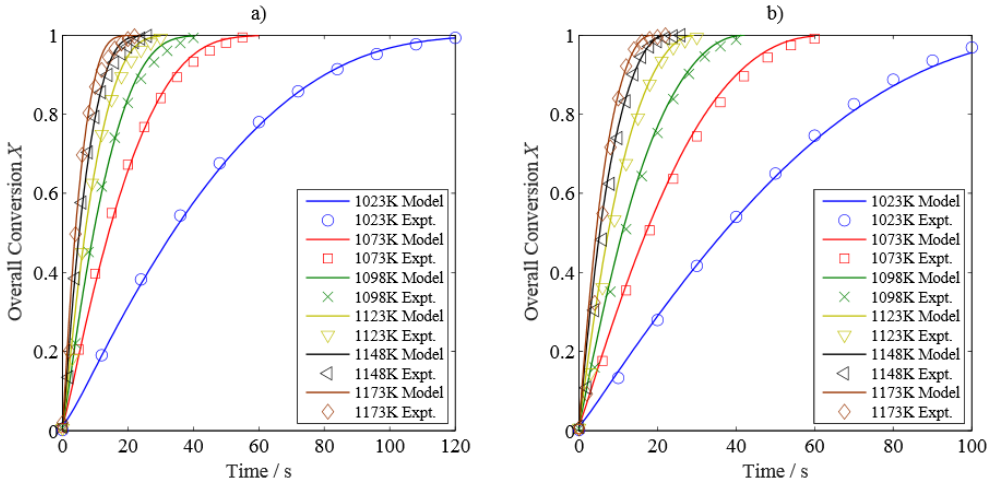

Fig. 9. Comparison of model results (lines) with experimental measurements (points) of the calcination of Purbeck limestone particles (6 cycles) by 100% N_2: a) 0.71 – 0.85 mm; b) 1.40 – 1.70 mm. The $f(X)$ determined from Compostilla 710 – 850 μm particles at 1073 K was used here.

Given the results, it can be concluded that using a constant $f(X)$ across different temperatures gives a satisfactory agreement between the model and the measurements for both Compostilla and Purbeck limestone. The fact that the $f(X)$ obtained from measurements of Compostilla could be successfully applied to the modelling of Purbeck suggests that the two limestone particles experienced similar changes of internal morphology during calcination. One reason that could explain this is that both particles had been periodically cycled several times before the final calcination reaction, which could have reduced the variations in pore structures thus making the two types of limestone particles more similar in terms of internal morphology. In addition, after a number of calcination – carbonation cycles, the reactivity of the particles approaches an asymptotic value. It might also be the case that the internal pore structure had developed into an "asymptotic" stage, where the original variations in pore structures between the two limestones had become slight on cycling.

5 Discussion

The above research is concerned with limestone which has been successively calcined and carbonated several times. Experimentally, the observed activation energies for the calcination of cycled, carbonated material were reasonably close to values in the literature, lying between 160 and 210 kJ/mol [14,15,38–40] for the calcination of virgin limestones, being 175 ± 12 kJ/mol and 186 ± 5 kJ/mol, respectively, for the Compostilla and Purbeck. These values, being close to the standard enthalpy of calcination, +178 kJ/mol, suggest that the activation energy for the reverse, carbonation reaction is small, being ~ -3 kJ/mol for Compostilla and ~ +8 kJ/mol for Purbeck. Thus, the intrinsic rate of carbonation changes little with temperature in the range of the temperature studied in the paper. Zawadzki and Bretsznajder [41] found that the rate of carbonation varies linearly with the difference between the partial pressure of CO_2 and its equilibrium value at 328 – 368ºC, which suggested that the rate constant was the same for all temperature thus a zero activation energy of the carbonation rate. Nitsch [42] also concluded that the rate of carbonation has an activation energy close to zero as the rate versus partial pressure difference gave a single linear line for measurements at 800 – 850ºC. The same conclusions were also reached by Bhatia and Perlmutter [43] and Dennis and Hayhurst [14] for carbonation experiments at 823 – 998 K and 1073 – 1248 K respectively.

Comparing the reaction rates of both limestones in **Fig. 5** and **Fig. 8**, it can be seen that the reactivity of Compostilla is slightly lower than that of Purbeck for 0.71 – 0.85 mm dia. particles. In addition, **Table 2** shows that the mean pore diameter of Purbeck limestones is only ~1/3 of that of Compostilla limestones. With higher

reactivity and smaller pore diameter, Purbeck limestone is indeed expected to experience more significant effects of intraparticle mass transfer on observed rate of reaction.

An interesting result from this study was that the $f(X)$ function determined from the measurements on the Compostilla limestone has been applied successfully in modelling the conversion of the Purbeck limestone. This implies that the evolution of the pore structure of both limestone particles are similar during calcination. One hypothetical reason for this observation is related to the cycling process of the limestones, where the change of pore structure become more stable as number of cycles increases. In fact, a study of the sulphation rate of cycled lime particles showed that different limestones followed a very similar conversion *vs.* time evolution after 50 cycles [44], which indicates that the cycling process does affect how the pore structure evolves with conversion.

6 Conclusions

It has been proposed that a simple arbitrary function $f(X)$, determined from experimental measurements of rate *vs.* conversion in the kinetically-controlled regime, could be used in place of mathematical pore models to describe the evolution of pore structure during a reaction that is influenced by intra-particle gas mass transfer. A model has been constructed using the Cylindrical Pore Interpolation Model for intraparticle mass transfer, first order rate equations of calcination, the Stefan-Maxwell equations for external mass transfer and the equations of energy. The model was solved numerically by orthogonal collocation on finite elements in MATLAB. The predicted results were compared with experimental measurements conducted using two size fractions of Compostilla (after 8 cycles) and Purbeck (after 6 cycles) limestones.

The results have shown that for the calcination of limestones, the empirically-determined $f(X)$ can be successfully applied to predicting the conversion of particles of various sizes across different temperature. In addition, it was found that the $f(X)$ determined from Compostilla limestones was successful in predicting the conversion of Purbeck limestones, which indicated that the two limestones had similar evolution of pore structure during calcination. This observation was attributed to the hypothesis that the calcination – carbonation cycling process might have significantly reduced the difference in the pore structures of the limestone particles and made them more homogenous.

The significance of this research is that the $f(X)$ concept presents a simple solution in modelling the evolution of pore structures during reactions of particles. Instead of using complicated mathematical pore models, one could determine the $f(X)$ from the experiments used for kinetic studies. This idea could be further applied to many other gas-solid reactions that involve change of pore structures during reactions. One needs to be aware of

the influence of multiple types of active sites which could lead to incorrect predictions. However, multiple sites are also not reflected in most published pore models.

Acknowledgements

The authors would like to thank Felix Donat, Wenting Hu and Zlatko Saracevic from the Department of Chemical Engineering and Biotechnology University of Cambridge for their assistance with the experimental work, and Peng Dai's family for financial support. Belén González acknowledges the EU Research Fund for Coal and Steel (project number RFCR-CT-2012- 00008).

References

[1] O. Levenspiel, Chemical reaction engineering, 3rd ed., John Wiley & Sons, New York, 1999.

[2] M. Kawahata, P.L. Walker, Mode of porosity development in activated anthracite, Elsevier, 1963. doi:10.1016/B978-0-08-009708-4.50026-2.

[3] S.K. Bhatia, D.D. Perlmutter, A random pore model for fluid-solid reactions: I. Isothermal, kinetic control, AIChE J. 26 (1980) 379–386. doi:10.1002/aic.690260308.

[4] J. Szekely, J.W. Evans, A structural model for gas—solid reactions with a moving boundary, Chem. Eng. Sci. 25 (1970) 1091–1107. doi:10.1016/0009-2509(70)85053-9.

[5] M. Hartman, R.W. Coughlin, REACTION OF SULFUR DIOXIDE WITH LIMESTONE AND THE GRAIN MODEL., AIChE J. 22 (1976) 490–498.

[6] W. Liu, J.S. Dennis, D.S. Sultan, S.A.T. Redfern, S.A. Scott, An investigation of the kinetics of CO2 uptake by a synthetic calcium based sorbent, Chem. Eng. Sci. 69 (2012) 644–658. doi:10.1016/j.ces.2011.11.036.

[7] G.R. Gavals, A random capillary model with application to char gasification at chemically controlled rates, AIChE J. 26 (1980) 577–585. doi:10.1002/aic.690260408.

[8] G.A. Simons, M.L. Finson, The Structure of Coal Char: Part I—Pore Branching, Combust. Sci. Technol. 19 (1979) 217–225. doi:10.1080/00102207908946882.

[9] J. Khinast, G.F. Krammer, C. Brunner, G. Staudinger, Decomposition of limestone: The influence of CO2 and particle size on the reaction rate, Chem. Eng. Sci. 51 (1996) 623–634. doi:10.1016/0009-2509(95)00302-9.

[10] R.C. Everson, H.W.J.P. Neomagus, R. Kaitano, R. Falcon, V.M. du Cann, Properties of high ash coal-char particles derived from inertinite-rich coal: II. Gasification kinetics with carbon dioxide, Fuel. 87 (2008) 3403–3408. doi:10.1016/j.fuel.2008.05.019.

[11] S.L. Singer, A.F. Ghoniem, An Adaptive Random Pore Model for Multimodal Pore Structure Evolution with Application to Char Gasification, Energy & Fuels. 25 (2011) 1423–1437. doi:10.1021/ef101532u.

[12] P. Dai, J.S. Dennis, S.A. Scott, Using an experimentally-determined model of the evolution of pore structure for the gasification of chars by CO2, Fuel. 171 (2016) 29–43. doi:10.1016/j.fuel.2015.12.041.

[13] M.A. Saucedo, J.Y. Lim, J.S. Dennis, S.A. Scott, CO2-gasification of a lignite coal in the presence of an iron-based oxygen carrier for chemical-looping combustion, Fuel. 127 (2014) 186–201. doi:10.1016/j.fuel.2013.07.045.

[14] J.S. Dennis, A.N. Hayhurst, The effect of CO2 on the kinetics and extent of calcination of limestone and dolomite particles in fluidised beds, Chem. Eng. Sci. 42 (1987) 2361–2372. doi:10.1016/0009-2509(87)80110-0.

[15] F. García-Labiano, A. Abad, L.F. de Diego, P. Gayán, J. Adánez, Calcination of calcium-based sorbents at pressure in a broad range of CO2 concentrations, Chem. Eng. Sci. 57 (2002) 2381–2393. doi:10.1016/S0009-2509(02)00137-9.

[16] I. Barin, G. Platzki, Thermochemical data of pure substances, 3rd ed., VCH, Weinheim ; New York, 1995. doi:10.1002/9783527619825.

[17] C.Y. Wen, Y.H. Yu, A generalized method for predicting the minimum fluidization velocity, AIChE J. 12 (1966) 610–612. doi:10.1002/aic.690120343.

[18] K.B. Bischoff, Accuracy of the pseudo steady state approximation for moving boundary diffusion problems, Chem. Eng. Sci. 18 (1963) 711–713. doi:10.1016/0009-2509(63)85050-2.

[19] C.Y. Wen, NONCATALYTIC HETEROGENEOUS SOLID-FLUID REACTION MODELS, Ind. Eng. Chem. 60 (1968) 34–54. doi:10.1021/ie50705a007.

[20] R.B. Evans, G.M. Watson, E.A. Mason, Gaseous diffusion in porous media at uniform pressure, J. Chem. Phys. 35 (1961) 2076. doi:10.1063/1.1732211.

[21] L.B. Rothfeld, Gaseous counterdiffusion in catalyst pellets, AIChE J. 9 (1963) 19–24. doi:10.1002/aic.690090105.

[22] P. Schneider, Multicomponent isothermal diffusion and forced flow of gases in capillaries, Chem. Eng. Sci. 33 (1978) 1311–1319. doi:10.1016/0009-2509(78)85112-4.

[23] D. Arnošt, P. Schneider, Dynamic transport of multicomponent mixtures of gases in porous solids, Chem. Eng. J. Biochem. Eng. J. 57 (1995) 91–99. doi:10.1016/0923-0467(94)02900-8.

[24] J.B. Young, B. Todd, Modelling of multi-component gas flows in capillaries and porous solids, Int. J. Heat Mass Transf. 48 (2005) 5338–5353. doi:10.1016/j.ijheatmasstransfer.2005.07.034.

[25] J.Y. Lim, J.S. Dennis, Modeling reaction and diffusion in a spherical catalyst pellet using multicomponent flux models, Ind. Eng. Chem. Res. 51 (2012) 15901–15911. doi:10.1021/ie302528u.

[26] R. Bird, W. Stewart, E. Lightfoot, Transport phenomena, 2nd ed., John Wiley & Sons, Inc., New York, 2007.

[27] D. Green, R. Perry, Perry's chemical engineers' handbook, 8th ed., McGraw-Hill Professional, New York, 2007. doi:10.1036/0071422943.

[28] R.S. Cunningham, C.J. Geankoplis, Effects of Different Structures of Porous Solids on Diffusion of Gases in the Transition Region, Ind. Eng. Chem. Fundam. 7 (1968) 535–542. doi:10.1021/i160028a002.

[29] A. Zoia, C. Latrille, Estimating apparent diffusion coefficient and tortuosity in packed sand columns by tracer experiments, J. Porous Media. 14 (2011) 507–520. doi:10.1615/JPorMedia.v14.i6.40.

[30] A. Hayhurst, M. Parmar, Measurement of the mass transfer coefficient and sherwood number for carbon spheres burning in a bubbling fluidized bed, Combust. Flame. 130 (2002) 361–375. doi:10.1016/S0010-2180(02)00387-5.

[31] R. Jackson, Transport in porous catalysts, in: Chem. Eng. Monogr., Elsevier Scientific Pub. Co., New York, 1977.

[32] D. Alvarez, M. Peña, A.G. Borrego, Behavior of different calcium-based sorbents in a calcination/carbonation cycle for CO2 capture, Energy & Fuels. 21 (2007) 1534–1542. doi:10.1021/ef060573i.

[33] Y. Wu, J. Blamey, E.J. Anthony, P.S. Fennell, Morphological changes of limestone sorbent particles during carbonation/calcination looping cycles in a thermogravimetric analyzer (TGA) and reactivation with steam, Energy and Fuels. 24 (2010) 2768–2776. doi:10.1021/ef9012449.

[34] J.F. Davidson, D. Harrison, Fluidised Particles, Cambridge University Press, Cambridge, 1963.

[35] R.C. Darton, R.D. LaNauze, J.F. Davidson, D. Harrison, Bubble growth due to coalescence in fluidised beds, Trans Inst Chem Eng. 55 (1977) 274–280.

[36] A.N. Hayhurst, The mass transfer coefficient for oxygen reacting with a carbon particle in a fluidized or packed bed, Combust. Flame. 121 (2000) 679–688. doi:10.1016/S0010-2180(99)00178-9.

[37] P.W. Chang, B. Finlayson, Orthogonal collocation on finite elements, Math. Comput. Simul. 20 (1978) 83–92. doi:10.1016/0378-4754(78)90031-9.

[38] A.B. Fuertes, G. Marban, F. Rubiera, Kinetics of thermal decomposition of limestone particles in a fluidized bed reactor, Chem. Eng. Res. Des. 71 (1993) 421–428.

[39] R.H. Borgwardt, Calcination kinetics and surface area of dispersed limestone particles, AIChE J. 31 (1985) 103–111. doi:10.1002/aic.690310112.

[40] M.S. Murthy, B.R. Harish, K.S. Rajanandam, K.Y. Ajoy Pavan Kumar, Investigation on the kinetics of thermal decomposition of calcium carbonate, Chem. Eng. Sci. 49 (1994) 2198–2204. doi:10.1016/0009-2509(94)E0015-I.

[41] J. Zawadzki, S. Bretsznajder, Concerning the temperature increment of the rate of reaction in reactions of the type A(solid)= B-solid+C-gas, ZEITSCHRIFT FUR ELEKTROCHEMIE UND Angew. Phys. CHEMIE. 41 (1935) 215–223.

[42] W. NITSCH, UBER DIE DRUCKABHANGIGKEIT DER CACO3-BILDUNG AUS DEM OXYD, ZEITSCHRIFT FUR ELEKTROCHEMIE. 66 (1962) 703–708.

[43] S.K. Bhatia, D.D. Perlmutter, Effect of the product layer on the kinetics of the CO2-lime reaction, AIChE J. 29 (1983) 79–86. doi:10.1002/aic.690290111.

[44] B. Arias, J.M. Cordero, M. Alonso, J.C. Abanades, Sulfation rates of cycled CaO particles in the carbonator of a Ca-looping cycle for postcombustion CO2 capture, AIChE J. 58 (2012) 2262–2269. doi:10.1002/aic.12745.

Table 1

Table 1. Composition of the fresh limestones in wt%.

Component	Ca	Fe	Mg	Ni	Al	K	Mn	Si	S	Zr	Sr	Ti
Compostilla	89.70	2.50	0.76	0	0.16	0.46	0	0.07	0	0	0	0.37
Purbeck	97.67	0.49	0.61	0	0.21	0.09	0.14	0.65	0.11	0.05	0	0

Table 2

Table 1. Particle characterisation of fully carbonated limestones.

Limestone	BET analysis			Mercury intrusion porosimetry					
	BET area / m^2 g^{-1}	BJH volume / cm^3 g^{-1}	BJH adsorption mean pore diameter / nm	Porosity	Total pore area / m^2 g^{-1}	Total intrusion volume / cm^3 g^{-1}	Mean pore diameter / nm	Bulk density / kg m^{-3}	Tortuosity factor / -
Compostilla, 8 cycles	0.33	7.2×10^{-3}	72	0.16	0.46	0.070	608	2235	2.8
Purbeck, 6 cycles	1.58	9.9×10^{-3}	21	0.34	3.88	0.188	190	1811	2.1

Figure 1

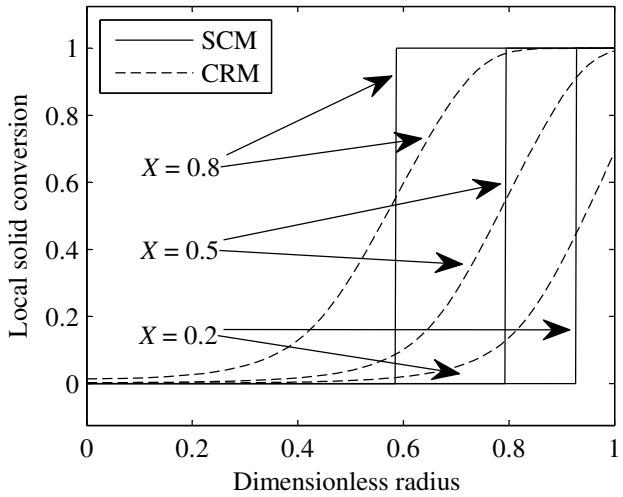
SCM
CRM
X = 0.8
X = 0.5
X = 0.2
Local solid conversion
Dimensionless radius
0
0.2
0.4
0.6
0.8
1

Figure 2

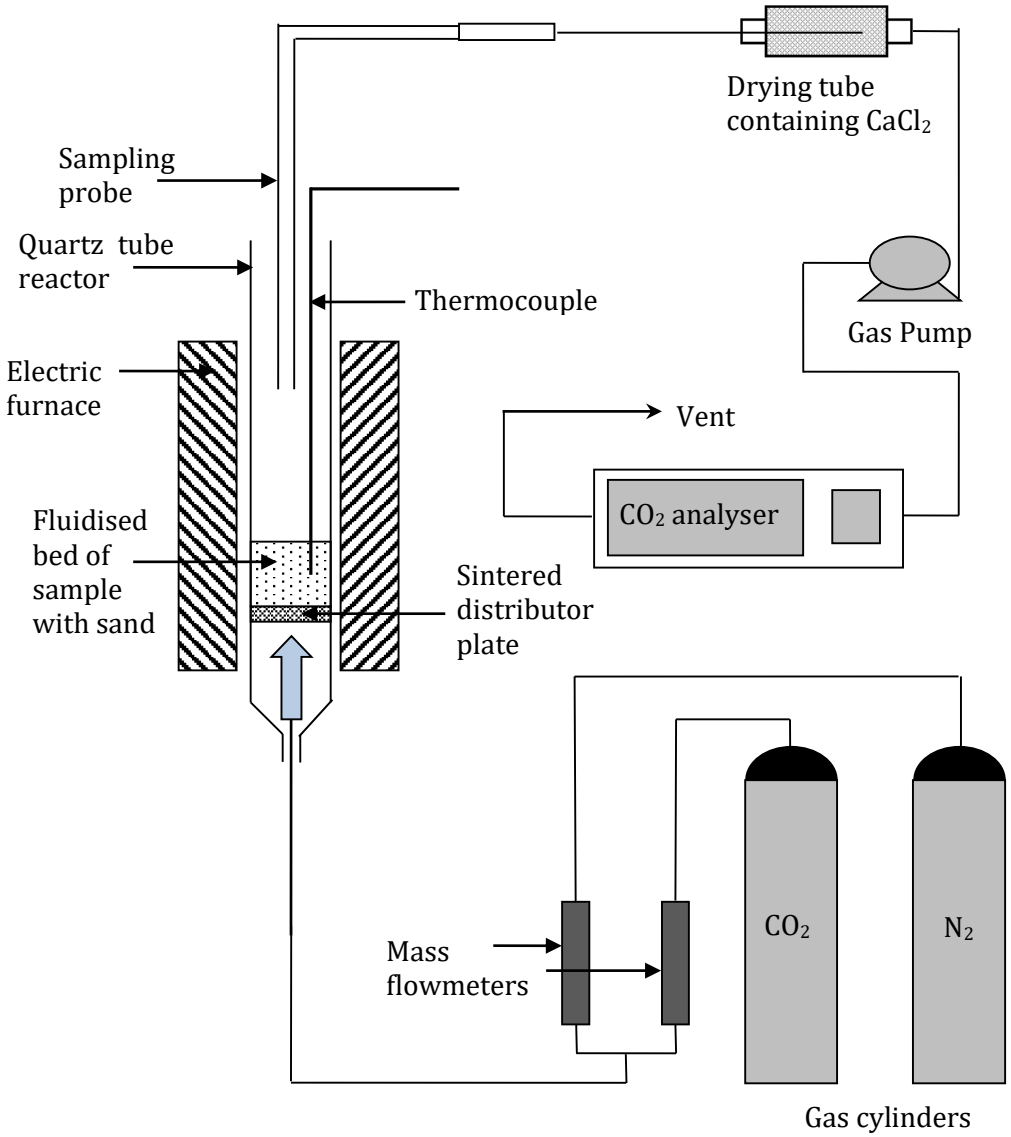
Drying tube containing $CaCl_2$
Sampling probe
Quartz tube reactor
Thermocouple
Gas Pump
Electric furnace
Vent
CO_2 analyser
Fluidised bed of sample with sand
Sintered distributor plate
Mass flowmeters
CO_2
N_2
Gas cylinders

Figure 3

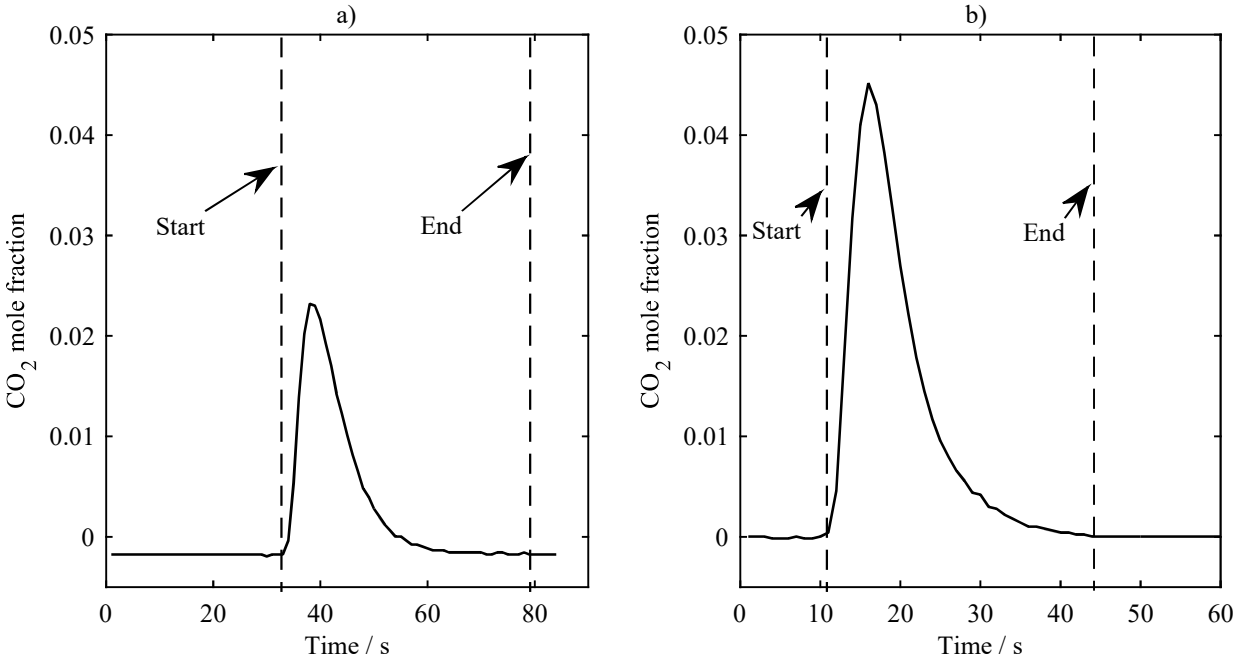
a)
b)
Start
End
Start
End
CO_2 mole fraction
CO_2 mole fraction
Time / s
Time / s
0.05
0.04
0.03
0.02
0.01
0
0
20
40
60
80
0
10
20
30
40
50
60

Figure 4

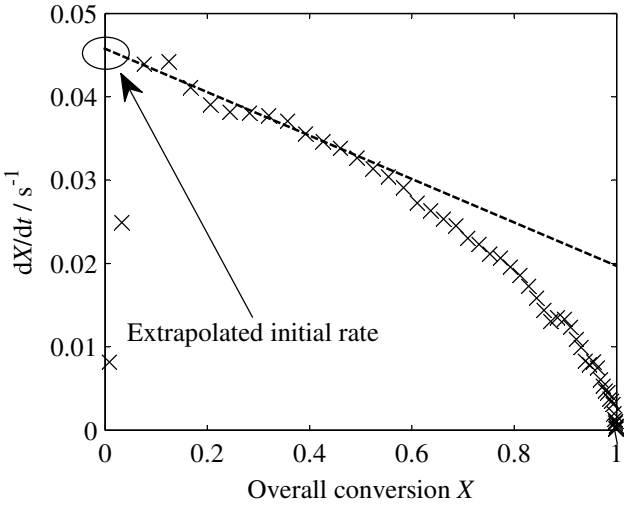
0.05
0.04
0.03
0.02
0.01
0
0
0.2
0.4
0.6
0.8
1
dX/dt / s-1
Overall conversion X
Extrapolated initial rate

Figure 5

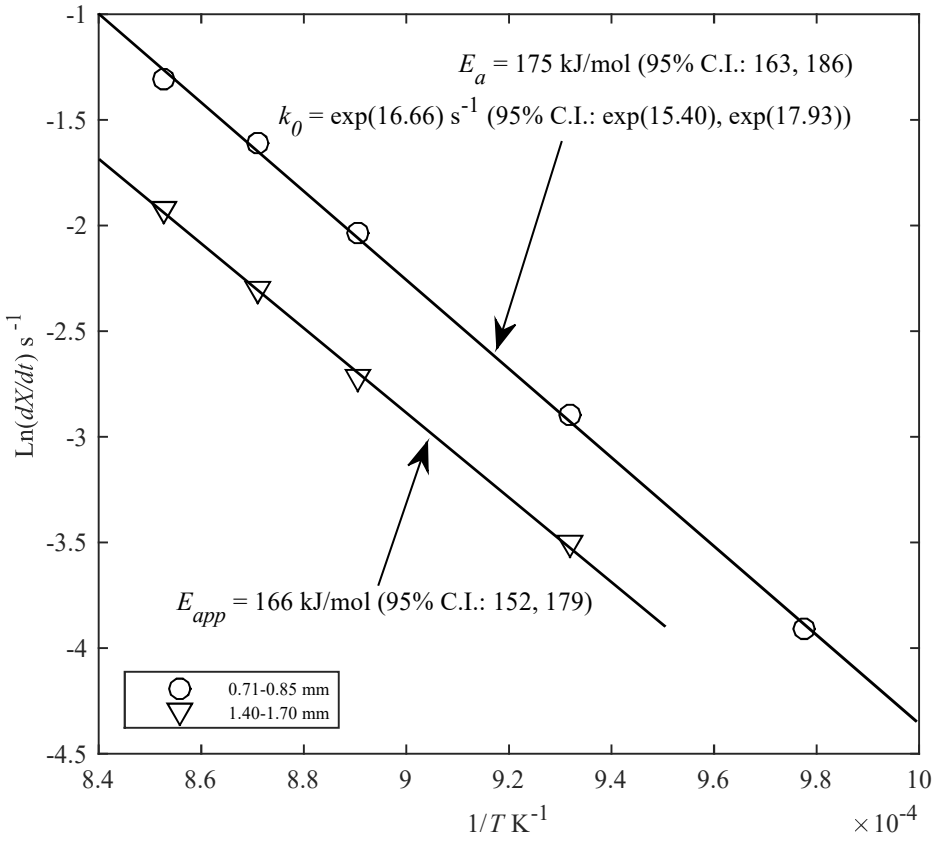
E_a = 175 kJ/mol (95% C.I.: 163, 186)
k_0 = exp(16.66) s^{-1} (95% C.I.: exp(15.40), exp(17.93))
E_{app} = 166 kJ/mol (95% C.I.: 152, 179)
0.71-0.85 mm
1.40-1.70 mm
Ln(dX/dt) s^{-1}
1/T K^{-1}
$\times 10^{-4}$
-1
-1.5
-2
-2.5
-3
-3.5
-4
-4.5
8.4
8.6
8.8
9
9.2
9.4
9.6
9.8
10

Figure 6

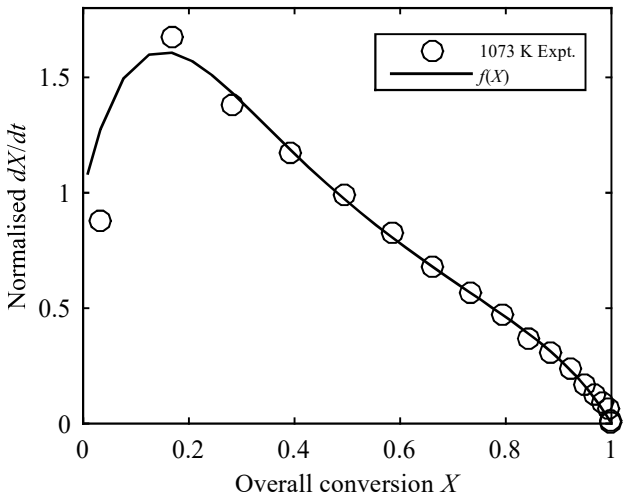
1073 K Expt.
f(X)
Normalised dX/dt
Overall conversion X
0
0.5
1
1.5
0
0.2
0.4
0.6
0.8
1

Figure 7

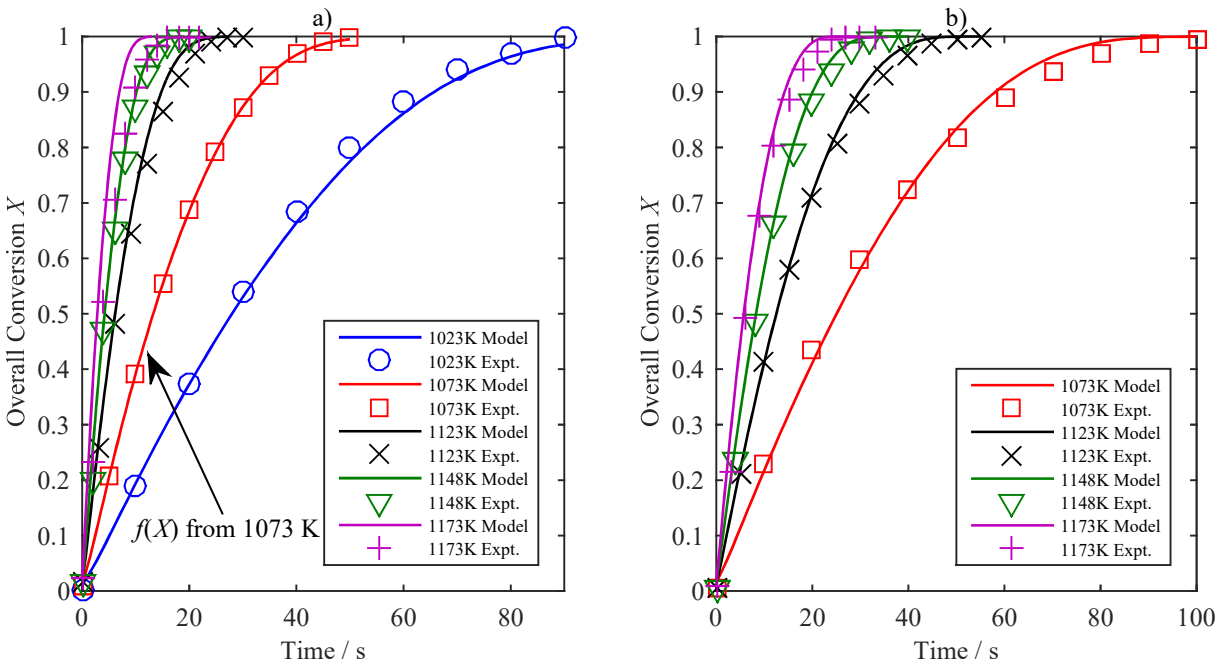
a)
Overall Conversion X
Time / s
$f(X)$ from 1073 K
1023K Model
1023K Expt.
1073K Model
1073K Expt.
1123K Model
1123K Expt.
1148K Model
1148K Expt.
1173K Model
1173K Expt.
b)
Overall Conversion X
Time / s
1073K Model
1073K Expt.
1123K Model
1123K Expt.
1148K Model
1148K Expt.
1173K Model
1173K Expt.

Figure 8

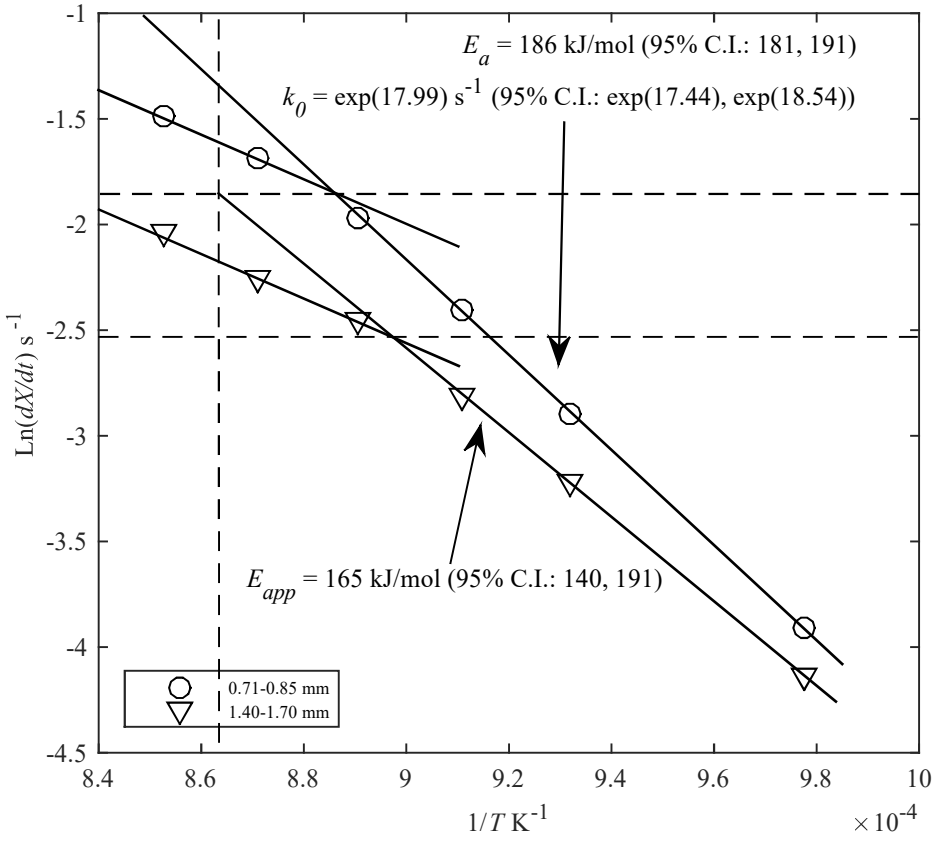
E_a = 186 kJ/mol (95% C.I.: 181, 191)
k_0 = exp(17.99) s^{-1} (95% C.I.: exp(17.44), exp(18.54))
E_{app} = 165 kJ/mol (95% C.I.: 140, 191)
0.71-0.85 mm
1.40-1.70 mm
Ln(dX/dt) s^{-1}
$1/T$ K^{-1}
$\times 10^{-4}$
-1
-1.5
-2
-2.5
-3
-3.5
-4
-4.5
8.4
8.6
8.8
9
9.2
9.4
9.6
9.8
10

Figure 9

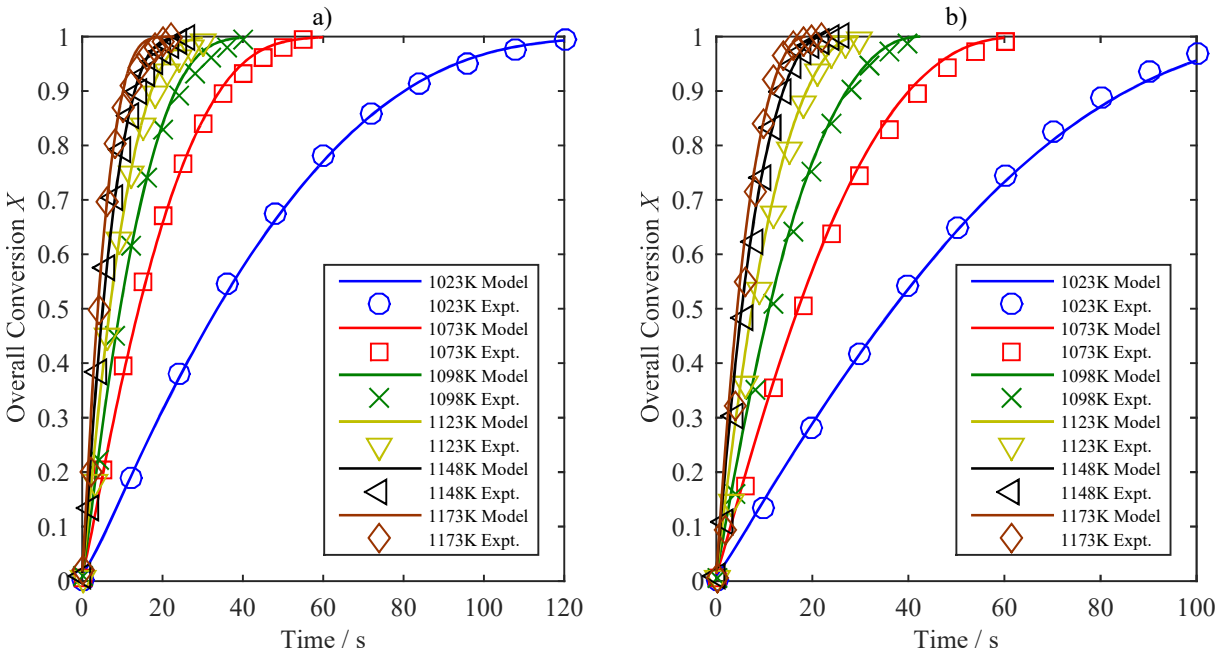
a)
b)
Overall Conversion X
Time / s
1023K Model
1023K Expt.
1073K Model
1073K Expt.
1098K Model
1098K Expt.
1123K Model
1123K Expt.
1148K Model
1148K Expt.
1173K Model
1173K Expt.

Figure 7 Supplementary MATLAB .fig files
Click here to download Supplementary MATLAB .fig files: FIG7.fig

Figure 9 Supplementary MATLAB .fig files

Click here to download Supplementary MATLAB .fig files: FIG9.fig